ATHENS UNIVERSITY OF ECONOMICS AND BUSINESS

ON THE INTERMITTENCY OF RAIN-FIELDS: A SPACE-TIME APPROACH

Harry Pavlopoulos and Vijay Gupta

Department of Statistics
Athens University of Economics and Business

Technical Report No. 143, May 2001

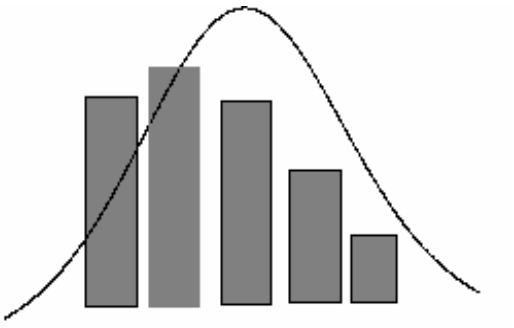

DEPARTMENT OF STATISTICS

TECHNICAL REPORT

ON THE INTERMITTENCE OF RAIN-FIELDS: A SPACE-TIME APPROACH

by

Harry Pavlopoulos[1,2*] and **Vijay Gupta**[2**]

[1] Department of Statistics
Athens University of Economics and Business
76 Patission Str., GR-10434 Athens, Greece

[2] Center for the Study of Earth from Space
Cooperative Institute for Research in the Environmental Sciences
University of Colorado
Campus Box 216, Boulder, CO-80309, USA

[*] *hgp@aueb.gr* (Corresponding author)

[**] *gupta@terra.colorado.edu*

Short Title: **Space-Time Intermittence of Rain-Fields**

Technical Report
May 2001

ABSTRACT

Most of the recent work on rainfall data analyses and modelling has focused on either its spatial or temporal variability. In this paper we investigate the structure of rainfall intermittence in space and time. Using a long series of TOGA-COARE radar scans converted to maps of pixel rain rate over a large tropical region of size $240 \times 240\ Km^2$, possible scale-invariant behavior of the probability distributions of dry and wet epoch durations are explored. Such durations are estimated by the lengths of dry and wet spells in time series of spatially averaged rain rate, over sampled square sub-regions of spatial scales ranging from 120 Km to 2 Km. The investigation is based on sample quantiles and sample moments of the underlying marginal probability distributions. We focus on the tail behavior of the probability distributions and investigate its variation with respect to spatial scale. Specifically, we find that the sample tail quantiles and sample moments of wet spells exhibit multiscaling of *power-law* type, while sample tail quantiles and sample moments of dry spells exhibit multiscaling of *exponential* type, across the range of the probed scales. These new findings, based on a rather wide range of spatial scales (120 Km to 2 Km), update, complement, and revise the findings of a recently published cadet study by the first author, in which wet and dry epoch durations of regional rainfall in the rather limited range of scales (10 Km to 2 Km) pointed to the possibility of simple scaling or self-similarity of such durations.

KEYWORDS: Intermittence; scale-invariance; dry and wet epoch durations; tail quantiles; statistical moments; spatio-temporal homogeneity.

1 Introduction

1.1 A conceptual framework

Rainfall is undoubtedly one of the most important facets of the global hydrological cycle, constituting a main link between the atmospheric circulation of ambient moisture and the river flows through the complex geomorphology of basins of drainage. Rainfall is manifested by clusters of events specified by the coordinates of their occurrence in space and in time, and also by their intensity or rain rate, which by integration over time and space quantifies *"how much"* rainfall water is accumulated *"where"* and *"when"* rainfall events occur.

This article is concerned with the fundamental feature referred to as *intermittence* of rainfall, a space-time feature indeed, since rainfall events are distinguishable over space, at any given instant of time, and are also distinguishable during time, at any given location of space. Given that rain rate is non-negative valued, rainfall intermittence may be defined more formally as being the *scheme of alternation* from zero to positive rain rate values and vice-versa. Such a formal scheme does not distinguish among positive values of rain rate, however high or low they may be, thusly being indifferent on the question of *"how much"* it rains. In this sense rainfall intermittence is concerned exclusively with the questions of *"where in space"* and *"when in time"* does it rain or does it not rain.

Rephrasing slightly these very questions to *"on how large a region in space"* and *"for how long a period in time"* does it rain or does it not rain, the present study tries to explore the possibility of a relationship between them, hence the *"space-time approach"*. The potential relationship is probed by sampling sub-regions $A \subseteq S$ of controlled size and shape from various locations within a fixed bounded "planar" region of study $S \subseteq \mathbb{R}^2$, and then by exploring possibilities of spatial scale-invariance of the spatial random processes of wet and dry epoch durations.

The spatial processes of wet and dry epoch durations are defined as follows. Given a sub-region $A \subseteq S$, consider the temporal random process $\{R_t(A)\ ;\ t \geq 0\}$ of spatially averaged rain rate over A, an intermittent process partitioned into wet epochs (i.e. spells of positive values) and dry epochs (i.e. spells of zeroes), whose lengths are assumed to be sample values from two random variables, W_A and D_A respectively. Thus, by varying the sampled sub-region $A \subseteq S$, one naturally obtains a spatial random process of wet epoch duration $\{W_A\ ;\ A \subseteq S\}$, and another spatial random process of dry epoch duration$\{D_A\ ;\ A \subseteq S\}$. It is also clarified that a sub-region $A \subseteq S$ is considered to be in a *dry epoch* for as long time as there is *nowhere* positive rain rate in it, so that the spatial average remains equal to zero, and it is considered to be in a *wet epoch* for as long time as there is *anywhere* or *somewhere* (but not necessarily everywhere) positive rain rate in it, so that the spatial average remains positive. That is, even if it rains only in very small or sparse patches over a given sub-region, and even there with very low (yet positive) rain rates, the sub-region is considered wet.

The concept of scale-invariance was introduced into studies of rainfields since nearly a decade and a half ago [Lovejoy and Mandelbrot (1985), Lovejoy

and Schertzer (1985), Schertzer and Lovejoy (1987), Waymire (1985)], and it has become a prominent framework within which variabilities in several aspects of rainfall in space and time may be unified, and also a new tool for statistical analyses of such aspects. The merit of scale-invariance, if it holds for some aspect of rainfall, is at least three-fold. Firstly, one may exploit relatively inexpensive and easily obtained information with respect to one scale, and use it under the proper scaling for inferences about the same aspect of rainfall in another scale of interest, within the range of scales where the invariance is valid. Secondly, stochastic modelling efforts for scale-invariant aspects benefit parsimony, at least in principle, since a reasonably satisfactory stochastic model obtained in one scale may also be of similar use in another scale, provided that its parameters are appropriately modified according to scaling. Thirdly, scale invariance of certain aspects of rainfall may be used as criterion for evaluating physical models of rainfall parametrization across certain ranges of scale in space or in time (e.g. downscaling of hydrometeorological variables based on General Circulation Model -GCM outputs).

Research efforts regarding scaling aspects of rainfall in space and time are reviewed by Foufoula-Georgiou and Georgakakos (1991), Foufoula-Georgiou and Krajewski (1995), and Foufoula-Georgiou (1998). Broader perspectives on the interrelations between scaling aspects of rainfall and issues of scaling in other branches of hydrological sciences are addressed in the books edited by Barndorf-Nielsen *et al.* (1998), Kalma and Sivapalan (1995), and Sposito (1998).

The most popular aspect of rainfall in studies exploring statistical scale-invariance, is its intensity or rain rate. Despite the various versions in which rain rate is usually treated in the pertinent literature (e.g. temporal averages, spatial averages, increments, power spectra over time or space, etc.), intermittence between rain and no rain is usually addressed merely indirectly, provided that the study is *not conditioned* on raining. Some recent examples of such studies in the space-time mode are given in works by Over (1995), Over and Gupta (1996), Harris (1997), Rodriguez-Iturbe *et al.* (1998), Pavlopoulos and Makatis (1998), Venugopal *et al.* (1999).

Our opinion is that there are other aspects of rainfall, via which space-time intermittence can be quantified, analyzed, and studied, more directly than via rain rate. We certainly consider wet and dry epoch durations of spatially averaged rain rate as being such an aspect, thusly worthy to study in this work, but there are other ones too. For example, time series of the fraction of wet (or dry) area over regions of various scales, as well as aspects of purely geometrical nature such as fractal dimensions of wet support over time and space. In fact, emphasizing the key importance of spatial random processes of wet and dry epoch durations for the study of space-time intermittence, we note that these processes can also be defined as lengths of wet and dry spells from time series of *wet area fractions* of the sampled sub-regions, without any knowledge of the exact rain rate values or of their spatial averages. Indeed, if $R_t(A)$ is interpreted as being the instantaneous fraction of wet area over a sampled sub-region $A \subseteq S$ at time $t \geq 0$, then the spells of zeroes and the spells of positive values in the temporally intermittent process $\{R_t(A)\ ;\ t \geq 0\}$ define exactly the same spatial processes $\{W_A\ ;\ A \subseteq S\}$ and $\{D_A\ ;\ A \subseteq S\}$ of wet and dry epoch durations as

before, when $R_t(A)$ denoted instantaneous spatial average of rain rate.

1.2 Objectives and related literature

To the best of our knowledge, the sole attempt to address spatial scaling properties of probability distributions of dry and wet epoch durations of spatially averaged rain rate, has been part of a recently published work by Pavlopoulos and Gritsis (1999). That work was primarily concerned with parametric modelling of probability distributions of such wet and dry durations. Scaling with respect to spatial scale, indicated through simple scaling of moments, was explored merely as extra statistical evidence, in addition to more conventional statistics for testing goodness of fit, supporting the inverse Gaussian family of probability distributions as a better model among other considered candidates. Notably, the same distribution model was also proposed by Freidlin and Pavlopoulos (1997), based on theoretical considerations regarding the physical mechanism of moisture budget. Although the work by Pavlopoulos and Gritsis (1999) points to the possibility of self-similarity or simple scale-invariance, it may be viewed as merely a cadet study in that direction, since the scales of the (square) regions over which the scaling was investigated were in a narrow range (from 10 Km to 2 Km), and therefore this very strong form of scaling may have been only circumstantial or incidental.

Another recent study, by Schmitt *et al.* (1998), addresses the probability distributions of dry and wet epoch durations, along with their conformity to the corresponding distributions obtained from modeling rain intensity via certain types of one-dimensional multifractal cascade models which do scale in a certain sense. That study addresses rainfall intermittence in the time domain only, using a 29-year long time series of rain intensity at a fixed *point location* (instead of averaging rain intensity mapped over a region), with high sampling frequency (every ten minutes). However, it does shed some light on the potential scaling behavior of dry and wet epoch duration distributions, and also on their connection with the dimension of the fractal set on which positive intensities are supported.

The present work aims primarily to a more thorough investigation of the possibilities for spatial scaling properties of probability distributions of wet and dry epoch durations of spatially averaged rain rate data, over regions whose sizes cover a much wider range of mesoscales from 120 Km to 2 Km. A formal definition of stochastic scale-invariance or stochastic scaling is given in Section 2, with its implications on the scaling behavior of quantiles and of existing moments, which in turn, under some assumptions of statistical nature, yield operational tools with which scaling becomes statistically tractable.. The part of TOGA-COARE data used in this study is explicitly described in Section 3, along with the formulation of our working data, while in Section 4 it is explained why the strategy of pooling data is preferred, along with statistical evidence supporting homogeneity assumptions needed for this strategy. The core of statistical analysis and results of our study are presented in Section 5, pointing to *power-law* scaling of sample tail-quantiles and of sample moments of wet spells, and to *exponential* scaling of sample tail-quantiles and of sample

moments of dry spells. These new findings point to a *multiscaling* behavior of the underlying spatial processes of dry and wet epoch durations, instead of simple scaling which was initially indicated in Pavlopoulos and Gritsis (1999). These findings are also associated with some of the results presented by Schmitt *et al.* (1998). Section 6 concludes with some remarks on the implications of the obtained statistical results, and with some thoughts for further research in those directions.

2 Formalism of scale-invariance and related aspects

2.1 Definitions, assumptions, and notation

Two sub-regions $A \subseteq S$ and $B \subseteq S$ will be called *geometrically similar* if they have identical shape, in the sense that each one of them is identifiable as a dilated or shrunk and possibly translated or rotated copy of the other. The ratio of diameters of two geometrically similar sub-regions defines the dimensionless *index of spatial scale* $0 < \lambda \leq 1$, so that if A is the larger of the two sub-regions, then the smaller one B may be *formally* denoted by $\lambda \cdot A$, although strictly speaking it is $\lambda \cdot A \neq B$, except when $B = \{\lambda \cdot \mathbf{x} \mid \mathbf{x} \in A\}$.

The practical purpose of the notation just introduced is to keep track merely of the relative size between two geometrically similar regions, ignoring all other aspects of relative position and orientation that distinguish two such regions. *That is, the notation $\lambda \cdot A$ refers indistinguishably to any sub-region (contained in S) which is geometrically similar to A and has diameter λ times smaller than the diameter of A.* In particular, A itself becomes indistinguishable from any translated or rotated copy of itself, since A may be also written formally as $1 \cdot A$. This interpretation of the notation $\lambda \cdot A$, combined with the assumptions of spatial and historical homogeneity postulated below, does facilitate a great deal in the statistical investigation of spatial scale-invariance (see Section 5).

Stochastic scale-invariance may be defined in a number of different ways, not necessarily equivalent. For the purposes of this study we recruit a rather standard and very basic definition, to say that the process $\{W_A \; ; \; A \subseteq S\}$ is *stochastically scale-invariant*, or *stochastically scaling*, with respect to the spatial scale $0 < \lambda \leq 1$, if there is a positive random function $\left\{C_\lambda^{(w)} \; ; \; \lambda \in (0,1]\right\}$, such that $C_1^{(w)} = 1$ with probability one, and for every $\lambda \in (0,1)$,

$$W_{\lambda \cdot A} \stackrel{L}{=} C_\lambda^{(w)} \cdot W_A \qquad (1)$$

or equivalently $W_{\lambda \cdot A} / C_\lambda^{(w)} \stackrel{L}{=} W_A$, in the sense of probability distribution functions. That is, the probability distribution of wet epoch duration W_A over any sub-region $A \subseteq S$, and the probability distribution of wet epoch duration $W_{\lambda \cdot A}$ over *the* sub-region $\lambda \cdot A = \{\lambda \cdot \mathbf{x} \mid \mathbf{x} \in A\} \subseteq S$, are linked through a *scaling factor* C_λ which is a random function merely of the spatial scale $\lambda \in (0,1]$, such that

$$P(W_{\lambda \cdot A} \leq u) = P(C_\lambda^{(w)} \cdot W_A \leq u) \qquad (2)$$

or equivalently $P(W_{\lambda \cdot A}/C_{\lambda}^{(w)} \leq u) = P(W_A \leq u)$, for every $u \in \mathbb{R}$ and every $\lambda \in (0,1]$. Indeed, these equations express a probabilistic relationship between the time-related question *"for how long a period does it rain"*, and the space-related question *"on how large a region does it rain"*. Of course, analogous is the definition of scale-invariance for the process $\{D_A \ ; \ A \subseteq S\}$, but then the probabilistic relationship would be between the time-related question *"for how long a period does it not rain"*, and the space-related question *"on how large a region does it not rain"*.

The degenerate case in which scale-invariance holds with $C_{\lambda}^{(w)}$ being a non-random scalar function, shall be referred to as *simple scaling* or *self similarity* of the process $\{W_A \ ; \ A \subseteq S\}$, and then necessarily $C_{\lambda}^{(w)} = \lambda^{\theta_w}$ is a power-law function of the scale λ, for some $\theta_w \in \mathbb{R}$ called *scaling exponent* of the self-similar process $\{W_A \ ; \ A \subseteq S\}$ (Lamperti 1962). The case of a scale-invariant process which is not self-similar (or simple scaling) shall be referred to as a *multiscaling* process (Gupta and Waymire 1990, 1993).

Now suppose that given a fixed sub-region $A \subseteq S$, and for each $\lambda \in (0,1]$, the notation $\lambda \cdot A$ does not stand strictly for *the* sub-region $\{\lambda \cdot \mathbf{x} \mid \mathbf{x} \in A\}$, but according to the earlier introduced interpretation it stands for any member of the class of sub-regions of S which are geometrically similar to A with diameter smaller than the diameter of A by the scale factor λ. Then, there is no conflict of this new interpretation of the notation $\lambda \cdot A$ in the definition of scale-invariance, as long as one is willing to assume that the probability distribution of wet (dry) epoch duration of spatially averaged rain rate is the same over any member of that class. Such an assumption clearly points to a notion of spatial stationarity (invariance under translations) and isotropy (invariance under rotations) of wet (dry) epoch durations over the region S, conditionally on the shape of $A \subseteq S$ and on the scale index λ of the test sub-regions sampled from the class $\lambda \cdot A$. This assumption is indeed adopted in the present study, and it is referred to as *spatial homogeneity* of wet (dry) epoch durations.

A second assumption made in this study is that the probability distribution of wet W_A (dry D_A) epoch duration over any fixed sub-region $A \subseteq S$, remains the same throughout the history of the process $\{R_t(A) \ ; \ t \geq 0\}$, or at least throughout the observed history $\{R_t(A) \ ; \ 0 \leq t \leq T\}$ up to time $T > 0$. This assumption is referred to as *historical homogeneity* of wet (dry) epoch durations, and it is under this assumption that it makes sense to say (see Introduction) that the lengths of all wet (dry) epochs in the history of $\{R_t(A) \ ; \ t \geq 0\}$ constitute a set of sample values from the random variable W_A (from the random variable D_A).

The third and last assumption made, is that the cumulative probability distribution functions (c.d.f.) of the positive random variables $W_{\lambda \cdot A}$ and $D_{\lambda \cdot A}$, defined respectively by $F_{\lambda \cdot A}^{(w)}(u) = P(W_{\lambda \cdot A} \leq u)$ and $F_{\lambda \cdot A}^{(d)}(u) = P(D_{\lambda \cdot A} \leq u)$, are continuous at every $u \in \mathbb{R}$, and strictly increasing over their common support $(0, +\infty)$. The role of this assumption is of rather technical nature, so as to guarantee that the corresponding *quantile functions*, generally defined for every $p \in (0,1)$ by $Q_{\lambda \cdot A}^{(w)}(p) := \inf\{u \in \mathbb{R} \mid F_{\lambda \cdot A}^{(w)}(u) \geq p\}$ and $Q_{\lambda \cdot A}^{(d)}(p) := \inf\{u \in \mathbb{R} \mid F_{\lambda \cdot A}^{(d)}(u) \geq p\}$, are also continuous and strictly increasing, and thusly coincide

with the inverse functions of the c.d.f.'s $F^{(w)}_{\lambda\cdot A}$ and $F^{(d)}_{\lambda\cdot A}$ (Karr 1993, p. 63). This helps in the simplification of the mathematical arguments connecting c.d.f.'s, quantile functions, and moments. Moreover, we believe that this assumption is also realistic from an intuitive and physical viewpoint, since there is no obvious reason of why one might exclude certain intervals of duration values from the support $(0, +\infty)$ of the c.d.f.'s (i.e. excluding strict monotonicity), or allow discrete probabilities attributed to certain duration values (i.e. allowing jump discontinuities).

For brevity, suppression of the superscripts (w) and (d) from the above notation indicates that the undergoing statement or argument refers without distinction to either wet, or dry epoch durations, or both. For example, n-th order moments are defined by

$$M_{\lambda\cdot A}(n) = \int_0^{+\infty} u^n dF_{\lambda\cdot A}(u) \qquad (3),$$

meaning that $M^{(w)}_{\lambda\cdot A}(n) = E\left(W^n_{\lambda\cdot A}\right) = \int_0^{+\infty} u^n dF^{(w)}_{\lambda\cdot A}(u)$ and $M^{(d)}_{\lambda\cdot A}(n) = E\left(D^n_{\lambda\cdot A}\right) = \int_0^{+\infty} u^n dF^{(d)}_{\lambda\cdot A}(u)$. Unlike c.d.f.'s and quantile functions, which always exist, n-th order moments exist only when the defining integral in (3) converges, and in that case all moments $M_{\lambda\cdot A}(k)$ of order $1 \leq k \leq n$ exist too. Moreover, under the assumption of continuity and strict monotonicity of c.d.f., when $M_{\lambda\cdot A}(n)$ exists it is possible to be calculated in terms of the corresponding quantile function $Q_{\lambda\cdot A}$ via the integral

$$M_{\lambda\cdot A}(n) = \int_0^1 \left[Q_{\lambda\cdot A}(p)\right]^n dp \qquad (4).$$

Equation (4) is obtained from (3), either by the change of variable $p = F_{\lambda\cdot A}(u)$ whence $Q_{\lambda\cdot A}(p) = Q_{\lambda\cdot A}(F_{\lambda\cdot A}(u)) = u$ for every $u \in \mathbb{R}$, or by the change of variable $u = Q_{\lambda\cdot A}(p)$ whence $F_{\lambda\cdot A}(u) = F_{\lambda\cdot A}(Q_{\lambda\cdot A}(p)) = p$ for every $p \in (0, 1)$.

2.2 Two hypothetical cases

If and when scale-invariance does hold, it is of great practical value for purposes of statistical inference to express scale-invariance explicitly in terms of c.d.f.'s most preferably, or in terms of quantiles if possible, or even in terms of moments if and when they exist. We illustrate this prospect for two specific hypothetical cases of scale-invariance. The one case is self-similarity, and the other is a particular case of multiscaling to which we refer as multiplicative cascade case, because of its obvious pertinence to scaling properties of multiplicative cascade processes (Holley and Waymire, 1992). In either case,and also in general, scaling expressed in term of moments, if they exist, is weaker than the notion of scaling expressed in terms of the corresponding quantile functions, while the latter notion is equivalent (under the constraints of continuity and strict monotonicity of c.d.f.) to our initial definition of scaling in terms of probability distributions.

2.2.1 Case of self-similarity

In the case of simple scaling or self-similarity of wet or dry duration processes, say with scaling exponent $\theta \in \mathbb{R}$, it follows directly from (2) that

$$F_{\lambda \cdot A}(u) = F_{1 \cdot A}(\lambda^{-\theta} \cdot u) = p \qquad (5),$$

whence, under the assumption of continuity and strict monotonicity of $F_{\lambda \cdot A}$ and $F_{1 \cdot A}$, it follows that $Q_{\lambda \cdot A}(p) = Q_{\lambda \cdot A}(F_{\lambda \cdot A}(u)) = u$ and $Q_{1 \cdot A}(p) = Q_{1 \cdot A}(F_{1 \cdot A}(\lambda^{-\theta} \cdot u)) = \lambda^{-\theta} \cdot u$, which by elimination of u yield

$$Q_{\lambda \cdot A}(p) = \lambda^{\theta} \cdot Q_{1 \cdot A}(p) \qquad (6).$$

Moreover, if $F_{1 \cdot A}$ admits finite moments up to order $n \geq 1$, then substitution of (5) into (3), or substitution of (6) into (4), yields that $F_{\lambda \cdot A}$ also admits finite moments up to order $n \geq 1$, and in fact for every $0 \leq k \leq n$,

$$M_{\lambda \cdot A}(k) = \lambda^{k \cdot \theta} \cdot M_{1 \cdot A}(k) \qquad (7).$$

2.2.2 Case of multiplicative cascade multiscaling

In the most general case of multiscaling of wet or dry duration processes, conditioning on the positive random variable C_λ (i.e. $C_\lambda^{(w)}$ for wet or $C_\lambda^{(d)}$ for dry) in the right-hand-side of (2), yields the equation

$$F_{\lambda \cdot A}(u) = \int_0^{+\infty} F_{1 \cdot A \mid C_\lambda}\left(\frac{u}{c} \mid c\right) dG_\lambda(c) \qquad (8),$$

where G_λ is the c.d.f. of the positive random variable C_λ, and $F_{1 \cdot A \mid C_\lambda}$ is the conditional c.d.f. of the wet duration variable W_A or of the dry duration variable D_A, given C_λ. The integral equation (8) is the multiscaling analogue of (5). Unfortunately, equation (8) is not reducible to a simple expression between the corresponding quantile functions, not even in the special case where C_λ is independent of W_A or D_A, a case in which conditioning would become a nuisance in (8).

However, in the case where the positive process $\{C_\lambda \ ; \ \lambda \in (0,1]\}$ is *independent* of W_A or D_A, following the line of argument given by Gupta and Waymire (1990, Section 4), it is seen that the underlying duration process $\{W_A; A \subseteq S\}$ or $\{D_A; A \subseteq S\}$ may admit a *multiplicative cascade representation*

$$W_{\lambda \cdot A} \stackrel{L}{=} W_A \cdot \exp\left\{Z^{(w)}_{\ln(1/\lambda)}\right\} \qquad \text{or} \qquad D_{\lambda \cdot A} \stackrel{L}{=} D_A \cdot \exp\left\{Z^{(d)}_{\ln(1/\lambda)}\right\} \qquad (9).$$

The corresponding process $\{Z_\alpha; \alpha \geq 0\}$, defined by $Z_\alpha = \ln C_{\exp(-\alpha)}$ for $\alpha \geq 0$, starts at zero with probability one (i.e. $P(Z_0 = 0) = 1$ since $P(C_1 = 1) = 1$), and has stationary (but not necessarily independent) increments in the sense that $Z_{\alpha_1 + \alpha_2} \stackrel{L}{=} Z_{\alpha_1} + Z_{\alpha_2}$ for every $\alpha_1 \geq 0$ and $\alpha_2 \geq 0$. The last equation is equivalent to $C_{\lambda_1 \cdot \lambda_2} \stackrel{L}{=} C_{\lambda_1} \cdot C_{\lambda_2}$, which follows directly from the definition of multiscaling of the underlying duration process, provided that the positive process $\{C_\lambda \ ; \ \lambda \in (0,1]\}$ is independent of W_A or independent of D_A. Note that

equations (9) accommodate also the degenerate cases of simple scaling where $P(Z_{\ln(1/\lambda)} = \theta \cdot \ln \lambda) = 1$.

A process which admits the multiplicative representation (9) is called *multiplicative cascade process*, and the corresponding scaling factor positive process $\{C_\lambda \ ; \ \lambda \in (0,1]\}$ is referred to as *factorial generator process* of the cascade. If the duration process $\{W_A; A \subseteq S\}$ or $\{D_A; A \subseteq S\}$ is indeed a multiplicative cascade process, then by taking moments up to order n (if they exist), and using once again the independence between $C_\lambda^{(w)}$ and W_A, or between $C_\lambda^{(d)}$ and D_A, equations (9) yield that for every $0 \leq k \leq n$,

$$M_{\lambda \cdot A}(k) = \Xi_\lambda(k) \cdot M_{1 \cdot A}(k) \qquad (10),$$

where $\Xi_\lambda(k) = E\left(\exp\left\{k \cdot Z_{\ln(1/\lambda)}\right\}\right)$ is the moment generating function (m.g.f.) of the random variable $Z_{\ln(1/\lambda)}$, hence a convex function. Equation (10) is a multiscaling analogue of (7), showing that k-th order moments are scaling not necessarily according to a simple power-law function of λ with exponent being a linear function $\theta \cdot k$ of the order k. Instead, moments in this multiscaling case scale according to the convex function factor $\Xi_\lambda(k) = \lambda^{S_\lambda(k)}$, where the exponent $S_\lambda(k) = \log_\lambda \Xi_\lambda(k) = \ln \Xi_\lambda(k) / \ln \lambda$ is a non-linear concave function of k, referred to as *structural function*, which may possibly depend on λ too.

Closing this section we should like to remark on the possibility of simple scaling in processes of wet and dry duration. This possibility relates subtly to the argument of Kedem and Chiu (1987), which rules out self similarity of rain rate processes in both space and time. Specifically, Kedem and Chiu (1987) showed that spatially averaged rain rate cannot be simple scaling with respect to spatial scale, because then the probability of rain (i.e. positive spatial average) ought to remain constant in all scales. However, this contradicts the empirical fact that the probability of rain is an increasing function of spatial scale. In the time domain, self-similarity of rain rate processes was also ruled out under the assumption of stationary increments, on the grounds that if it ever stopped raining, it would never restart. Therefore, the possibility of simple scaling was ruled out for rain rate processes on the grounds of their intermittence in space and time. However, although wet and dry durations of spatially averaged rain rate provide a space-time approach to studying rainfall intermittence, the possibility of their simple scaling cannot be ruled out on the basis of the above argument, at least not a priori, for the very simple reason that they are always strictly positive processes, thus not intermittent ones.

3 Formulation of working data from TOGA-COARE measurements

The source of raw data used in this study is a set of maps of radar reflectivity measurements, obtained during the Tropical Ocean Global Atmosphere (TOGA) Coupled Ocean-Atmosphere Response Experiment (COARE), from two shipborne Doppler precipitation radars (TOGA and MIT) scanning every ten minutes a large tropical region of approximate size $300Km \times 400Km$ in

the China Sea, off the north coast of Australia. The duration of this field experiment was approximately three months (November 1992 through January 1993), divided into three main phases known as Cruise 1, Cruise 2, and Cruise 3. Reflectivity measurements from each scan or snapshot were binned over small square pixels of size 2×2 Km^2 each, whence instantaneous rain rate values were obtained using the so-called Z-R relationship $R = (Z/230)^{1/1.25}$ between reflectivity Z and rain rate R. Detailed information about TOGA-COARE can be found in Short *et al.* (1997).

The part of TOGA-COARE data available to us for this study covers only a square sub-region of size 240x240 Km^2, with a temporal resolution of approximately 20 minutes between successive scans, consisting of 1992 scans from Cruise 1 (November 10, 1992 through December 9, 1992) and of 617 scans from the early part (December 21, 1992 through December 29, 1992) of Cruise 2. There is also a small number of missing scans, making up 48 blocks of missing scans in Cruise 1, and 21 blocks in Cruise 2. Most of these blocks, percentage 87%, consist of one or two missing scans (per block), while the longest block in Cruise 1 consists of 18 missing scans (i.e. about six hours), and the longest block in Cruise 2 consists of 6 missing scans (i.e. about two hours). Figure 1 depicts the instantaneous rain rate field retrieved from a typical scan of Cruise 1.

3.1 Spatial sampling design

By computing the spatial average of rain rate over all pixels in each scan, two time series were obtained, for Cruise 1 and Cruise 2 respectively. Apart from a few blocks of missing values, whose time coordinates are exactly those of blocks of missing scans, the rest of the values in each one of these time series are positive. This showed that at the spatial scale of 240 Km it "always" rained somewhere in the probed region, and therefore this spatial scale is not informative about durations of dry and wet spells. Consequently, time series of spatially averaged rain rate at scales smaller than 240 Km were explored, so as to start having enough temporal intermittence in order to be able to obtain sufficient statistical information about duration (or length) of dry and wet spells. The desired temporal intermittence started to appear in a fairly robust manner at scales not larger than 120 Km, and for this simple reason we conventionally associate that scale with the dimensionless value $\lambda = 1$, considering it as *scale of reference* hereafter. Figure 2 depicts a fixed sampling design of five (geometrically similar) square sub-regions, which are used as test sub-regions at the scale of reference, each one consisting of $60 \times 60 = 2400$ contiguous pixels. Four of these sub-regions (NW, NE, SW, SE) partition the probed region of study, while the central one (CR with dashed borders) intersects symmetrically each one of the four disjoint compartments.

Other spatial scales treated in this study are those obtained from an approximate *"rule of half"*, applied sequentially six times on the scale of reference, down to the scale of a single pixel. These scales correspond to 60 Km ($\lambda = 60/120 = 1/2$), 30 Km ($\lambda = 30/120 = 1/4$), 16 Km ($\lambda = 16/120 = 2/15$), 8 Km ($\lambda = 8/120 = 1/15$), 4 Km ($\lambda = 4/120 = 1/30$), and 2 Km ($\lambda = 2/120 =$

1/60), and together with the scale of reference outline a rather wide range of mesoscales being of particular interest for both meteorological (e.g. downscaling of GCM output) and hydrological (e.g. river basin flows and flood frequency analysis) applications. Test sub-regions from each one of the treated scales are selected from each sub-region of Figure 2, according to the five sampling designs depicted in Figure 3. For example, the NW design in Figure 3 applied to the SE sub-region of reference scale in Figure 2, samples six square sub-regions nested within one another along the diagonal towards the NW vertex of the SE sub-region of reference. In short, this system of seven sampled sub-regions is denoted by SE-NW, indicating that the SE sub-region of reference scale was sampled first, followed by six nested sub-regions "tied" to its NW vertex.

Obviously there are numerous alternatives of defining sampling designs other than the one just described. Our main reason for considering this particular sampling mechanism, is that due to its symmetry it covers quite densely and in a rather economic manner the entire probed region (240x240 Km^2) in all seven scales treated in this study, providing statistical information (about dry and wet durations) from 25 different test sub-regions for each one of the six smaller scales (60 Km, 30 Km, 16 Km, 8 Km, 4 Km, 2 Km), and from 5 different test sub-regions of the reference scale (120 Km). Moreover, this particular sampling scheme keeps spatial overlaps as minimal as possible among test sub-regions of the same scale. The benefit from minimal overlapping is that repetitious information, from test sub-regions which are nearly the same, is avoided to a large extent. This in turn simplifies the statistical inference and facilitates the interpretation of results.

3.2 Pooling of statistical information

The sampling scheme described above, produces a total number of 155 different sub-regions (i.e. 5x1 + 25x6) of the probed region, whence statistical information about dry and wet epoch durations is obtained and analyzed in Section 4 in order to explore if there is any scaling behavior and of what kind.

The first step in that direction was to obtain the time series of spatially averaged rain rate corresponding to each one of the 155 sub-regions. Blocks of zeros and blocks of positive values, appearing in alternating sequence, correspond to dry and wet spells respectively, occasionally interrupted by a block of missing values. Sample values of wet (dry) epoch durations were estimated by the corresponding number of measurements in each spell, called *length of the spell*. Obviously, lengths of wet and dry spells are positive integers, which if multiplied by the temporal sampling frequency 1/3 hr express the sample values of wet and dry durations in units of hours (hr). Although this is a natural way to estimate wet and dry epoch durations, it is also rather crude because it assumes that there was no temporal intermittence during any 20 minute sampling interval, which clearly may be untrue especially over regions of small size. Moreover, wet and dry spells bordering with a block of missing values in a time series were just discarded, because they obviously are another source of ambiguity for the true length of a few dry or wet spells. Serving as an example, Figure 4 depicts the time series of spatially averaged rain rate during Cruise 1,

over the seven nested sub-regions sampled by the NE-CR design.

The second step was to pool lengths of wet spells from Cruise 1 and Cruise 2, retaining chronological sequence of spell lengths within each cruise and also between cruises, and the same sort of pooling was applied also to lengths of dry spells. This procedure is hereafter referred to as *temporal pooling* of wet or dry spell lengths, and it was applied on each one of the 155 test sub-regions.

The third step was to pool the temporally pooled wet spell lengths from all test sub-regions of the same scale, so as to obtain one data set of wet spell lengths for each one of the seven spatial scales. This procedure is hereafter referred to as *spatial pooling*, and of course it was also applied to temporally pooled lengths of dry spells from all test sub-regions of each scale.

After temporal and spatial pooling, the final product consists of 7 pools of wet spell lengths, and another 7 pools of dry spell lengths. These final 14 spatio-temporal pools (two pools, dry and wet, for each one of the seven scales) constitute our *working data* for the purposes of this study.

4 Justification of pooling and homogeneity

The target task being the statistical investigation of scaling possibilities regarding the probability distributions of wet and dry epoch durations, with respect to the spatial scale of the sampled sub-regions, is carried out in Section 5 considering sample tail-quantiles and sample moment estimates of the underlying probability distributions. However, before going into the details of that analysis, some justification should be given for our choice of strategy to work with spatio-temporally pooled spell length data, hereafter called *pooled strategy*. The obvious alternative would be to carry out the same analysis separately for each individual system of nested sub-regions, maintaining temporal pooling per sub-region, but without spatial pooling of data from regions of the same scale from different systems. This alternative is called *individual strategy* hereafter.

Under the individual strategy, scaling analysis of quantiles and moments ought to be performed separately on each one of the 25 systems of nested sub-regions obtained by the implemented spatial sampling designs. Subsequently, conclusions ought to be drawn based on some summary statistics of scaling exponents and the like parameters quantifying whatever forms of scaling behavior might emerge. Such strategy would not require the assumption of spatial homogeneity, but only that of historical homogeneity. Nevertheless, a serious shortcoming of that strategy is that inference for lower and mid-range quantiles is severely obscured by the extremely prominent skewness of the data, and by the same token inference for upper-tail quantiles would have be based only on very few and sparse extreme values in samples whose sizes at best are in the order of only a few decades. A glimpse of this situation is given in Figure 5, presenting statistical summaries in the form of box-plots for wet and dry epoch durations in all seven scales, obtained after temporal pooling applied to the individual system of seven nested sub-regions sampled by the NE-CR design. Note that due to the temporal pooling between Cruise 1 and Cruise 2 over each sub-region, sample sizes are slightly higher than those marked in the Cruise 1

time series plots depicted in Figure 4, yet the above described shortcomings are quite obvious.

Under the pooling strategy the situation improves partially, in the sense that, although extremely high skewness prevails also in the spatio-temporally pooled working data at each scale, hence still obscuring statistical inference about lower and mid-range quantiles, inference about upper-tail quantiles becomes more feasible and robust due to the gain of information about the extreme values of the underlying probability distributions from substantially larger samples. Figure 6 depicts this improvement via boxplots corresponding to all seven spatial scales treated, after spatial pooling.

Indeed, comparing the box-plots in Figure 6 with those in Figure 5, it is obvious that in all spatial scales, both dry and wet spell lengths are highly skewed, with a very short interquartile range whose upper end does not exceed the 2 hours, except in the 4 Km dry and the 60 Km wet cases where the corresponding sample upper quartiles are nearly 2.3 and 3.3 hours respectively. However, the gain of information about extreme values higher than the upper quartile is quite substantial, except for the 120 Km scale where there is not much improvement after spatial pooling (recall that there are only 5 samples pooled for this scale, instead of 25 samples for every other scale). It is noted that the NE-CR design is one of the most informative among the 25 designs considered in the study (see again the NE quarter of the study region in Figure 1), and for this reason it has been chosen for comparison with the pooled working data sets.

Sample quantile estimates for specific values across the range (0,1) of probability levels (including the probability levels 0.25 and 0.75 for the lower and upper quartiles respectively) are given in Table 1 for the spatio-temporally pooled working data, whence it becomes strikingly clear that scaling analysis of quantiles is feasible only for upper-tail quantiles, say for probability levels higher than 0.75. Indeed, for probability levels lower than 0.75, sample quantiles across the different spatial scales become almost indistinguishable as they collapse to only a couple of different values (say 2 and 3 for the 0.55 level), thus making impossible the study of any scaling structure however prominent or subtle it may be, if it holds at all. This masking effect is indeed rather annoying, and it is easily attributable partly to the prominent skewness of the underlying probability distributions, and partly to the rather long sampling frequency of 20 minutes which "quantizes" the data.

Choosing the pooling strategy instead of the individual strategy, for the reasons explained above, bears the additional cost of having to adopt also the assumption of spatial homogeneity (see section 2.1), along with the assumption of historical homogeneity which is needed for justification of either strategy. One might be convinced to accept both these homogeneity assumptions on the basis of some general intuitive argument addressing in loose qualitative terms the physical mechanism responsible for setting on and off the occurrence of rainfall events over space and time. For example, such an argument might imply the desired statistical homogeneity from a broad sense of climatic stability and uniformity over the probed geographical region (e.g. tropical in this study) during a specific season (e.g. monsoon season in this study). However, since

these two homogeneity assumptions are of fundamental importance for the task of scaling analysis in this study, especially under the pooling strategy, some additional effort was made in order to address in a more quantitative manner the potential validity of these assumptions via some statistical tests.

4.1 Evidence of historical homogeneity

In order to test homogeneity during time, the non-parametric test of runs above and below the median was applied for every individual sub-region from each scale, after temporal pooling of the corresponding information from both Cruise 1 and Cruise 2. In fact, this testing procedure tests not only homogeneity of the parent probability distribution (of the temporally pooled data per sub-region), but the stronger null hypothesis that the data constitute a random sample of observations from independent and identically distributed (i.i.d.) random variables. This testing procedure is actually a ramification of the well known Wald-Wolfowitz asymptotic test, requiring large enough samples so that both scores of runs above and below the median are large too, and it is described with some detail in Pavlopoulos and Gritsis (1999, section 2.2).

The evidence provided by these tests is measured by the corresponding p-values (or significance probabilities), whose box-plot summaries per spatial scale (except the scale of reference) are given in Figure 7 for both dry spell lengths (top row) and wet spell lengths (bottom row). In particular, quantiles at the 0.1 probability level of the obtained p-values are all higher than 0.01, meaning that, in at least 90% of the sampled sub-regions of any given scale, the i.i.d. null hypothesis for either wet or dry spell lengths is accepted with confidence 99%. Indeed, this constitutes quite satisfactory evidence in support of the null hypothesis of i.i.d. observations, hence also of the historical homogeneity assumption in every scale, for wet epoch durations as well as for dry. In fact, more attentive reading of Figure 7 indicates that the evidence is slightly stronger for wet spells than for dry.

Box-plots of p-values for the scale of reference (120 *Km)* are not included in Figure 7, because at that scale there are only 5 p-values (instead of 25 for each of the other six scales), which are also hard to interpret since the corresponding sample sizes are too small for the asymptotic test used (between 3 and 21 for dry, and between 2 and 13 for wet spell lengths).

4.2 Evidence of spatial homogeneity

Testing for spatial homogeneity refers to testing, in each fixed scale, for invariance of the underlying probability distribution (of the already temporally pooled data, of dry and wet spell lengths separately), among the sampled sub-regions of that scale.

The test of runs above and below the median may be applied again, although it is not quite appropriate since spatially pooled data no longer reflect any chronological sequence in which they were observed, and therefore the statistical significance of the null hypothesis of randomness varies according to the permutation of blocks of data from the different sub-regions of the same scale

(chronological sequence is however maintained within each block since it consists of the temporally pooled data over a specific sub-region). Despite these drawbacks, this testing procedure is somewhat informative, in the sense that under different permutations, although p-values do vary indeed, it appears that the null hypothesis of randomness is not rejectable over the larger scales (120 Km - 16 Km for wet spells, and 120 Km - 30 Km for dry spells), but it is rejectable over the smaller scales.

Retaining the above mentioned reservations regarding appropriateness of this testing procedure, the results are not all that discouraging about the validity of spatial homogeneity, as the rejection of the null hypothesis of randomness may be attributed to the presence of some spatial dependence and not to lack of spatial homogeneity. This last point is supported also by the fact that when the test was applied to spatially pooled data from only disjoint sub-regions of the same scale, p-values did increase slightly, especially for spatially pooled dry data.

To shed more light on the question of spatial homogeneity of dry and wet spells from different sub-regions of a given scale, further classical statistical tests of homogeneity were employed, namely the Kruskal-Wallis test, and the χ^2-homogeneity test. Both these testing procedures allow for comparison between several (temporally pooled) samples of wet (or dry) spell lengths, one sample from each sampled sub-region of a given scale. Both these non-parametric asymptotic tests require independent large samples, not necessarily of the same size, each sample consisting of i.i.d. data. From these two requirements, the latter is evident enough on the basis of temporal randomness, but the former is evidently not met due to spatial dependence between samples from different sub-regions of the same scale. Moreover, we note that the χ^2-homogeneity test was difficult to apply, because of the high skewness in each sample, often yielding unavoidably low scores (below 5 and even 0 sometimes) in some partitioning cells.

Despite these shortcomings regarding appropriateness and applicability of the Kruskal-Wallis test and of the χ^2-test in the situation at hand, merely explorative application of them yields similar results to those obtained from the test of runs above and below the median. Namely, spatial homogeneity is supported at larger scales (120 Km - 16 Km for wet spells under both tests, and 120 Km - 60 Km for dry spells only under the χ^2-test).

In light of the above remarked shortcomings of testing homogeneity *simultaneously* among samples from all sampled sub-regions of the same scale (5 for the reference scale and 25 for every other scale), one may resort to testing merely *pairwise* independence and homogeneity in each pair of samples from the sampled sub-regions of the same scale. To this end, a battery of nonparametric asymptotic tests may be used, namely Kolmogorov-Smirnov, Wilcoxon-Mann-Whitney (a two-samples analogue of the Kruskal-Wallis test), and χ^2-test for testing homogeneity, and Spearman's rank-correlation, Kendall's τ-test, and χ^2-test for testing independence. The p-values of these tests of independence are indicative of the appropriateness of the tests for pairwise homogeneity, since each of the homogeneity tests presumes independence between the two compared samples (along with randomness within each sample, which has already

been accepted). Detailed descriptions of these tests are given in standard statistical books, such as Bickel and Doksum (1977), Lehmann (1986), Rao (1973), and Rohatgi (1976).

Although pairwise independence is much weaker than, and certainly not equivalent to mutual independence among the individual random samples from all subregions of the same scale, pairwise independence does provide an alternative approach towards testing global homogeneity. That is, one may resort to evidence of independence among random samples from pairs of subregions of the same scale, in order to justifiably apply the above mentioned homogeneity tests to each of those very pairs of independent random samples. Furthermore, one may argue that if homogeneity is evident among pairs of independent random samples, then this very pairwise homogeneity can be considered as reasonable evidence of global homogeneity among the individual random samples from all subregions of the same scale. In other words, evidence of pairwise independence and of pairwise homogeneity thereafter, render global homogeneity plausible, even when lack of mutual independence (attributed to some spatial dependence) disables testing for global homogeneity directly in a single trial.

Clearly, there are $\binom{5}{2} = 10$ pairs of (temporally) random samples of wet (dry) spell lengths for the reference scale and $\binom{25}{2} = 300$ pairs of such random samples for each of the other six scales. The seven tests mentioned above (three for pairwise independence and four for pairwise homogeneity) were applied on several pairs of sampled sub-regions from each scale, but certainly not on all of them, The obtained p-values from each test applied to different pairs of sub-regions of the same fixed scale, showed some variability but were always supportive of the null hypothesis tested (pair independence or pair homogeneity). For this reason, and also due to space limitations, summary statistics of p-values from each given test applied to several pairs of a given scale, have been intentionally omitted.

Instead, we consider much more interesting to have a glimpse on the variability of p-values from the entire battery of tests when applied across the various spatial scales. Table 2 serves this purpose, tabulating p-values obtained from all seven tests applied on pairs of samples of wet spell lengths, and also on pairs of samples of dry spell lengths, corresponding to the pairs of sub-regions sampled in each scale by the NW-CR and NE-CR sampling designs. Quite similar p-values were also obtained in all the other pairs of sampling designs that we tried, namely NE-CR & SE-CR, SE-CR & SW-CR, SW-CR & NW-CR, SW-CR & NE-CR, NW-CR & SE-CR, and a few more.

The empirical conclusions which can be drawn from the pairwise approach towards testing global homogeneity per scale, to the extent that it was actually explored, can be summarized as follows. Regarding pairwise independence, all three tests (χ^2, and Kendall's and Spearman's correlation tests) yield quite large p-values, supporting the statistical significance of pairwise independence, among pairs of wet duration samples as well as among pairs of dry duration samples, in every spatial scale. Consequently, this constitutes evidence that all the homogeneity tests (χ^2, Kolmogorov-Smirnov, Wilcoxon-Mann-Whitney, and Kruskal-Wallis) are appropriate to use for further testing of pairwise ho-

mogeneity. Indeed, all four tests yield quite large p-values too, providing rather convincing evidence in favor of accepting pairwise homogeneity in every spatial scale, among samples of wet spell lengths and also among samples of dry spell lengths. Therefore, in light of the argument given earlier, we shall consider the available evidence satisfactory enough so as to adopt hereafter the postulated global spatial homogeneity assumption.

5 Scaling analysis

Core of the scaling analysis undertaken in this section is the statistical investigation of the theoretical relationships expressed by equations (6), (7), and (10). These relationships are considered merely as certain basic forms of scaling, certainly not exclusive of other possibilities, and any significant departures thereof ought to be interpreted as evidence of other forms of scaling associated with model processes other than the two hypothetical ones presented in Section 2.

The actual practice of these investigations consists of simple linear regressions of $\ln\{q_\lambda(p)/q_1(p)\}$ and of $\ln\{m_\lambda(k)/m_1(k)\}$ on the spatial scale λ or on $\ln\lambda$, and on the statistical significance of the corresponding regression coefficients, and their behavior as functions of p and k respectively. The notation $q_\lambda(p)$ stands for sample estimates of quantiles $Q_\lambda(p)$ at probability level $p \in (0,1)$, and the notation $m_\lambda(k)$ stands for sample estimates of moments $M_\lambda(k)$ of order $k > 0$ up to the order for which moments are assumed to exist.

For the reasons addressed in Section 4, scaling analysis of sample quantiles $q_\lambda(p)$ focuses merely on tail-quantiles corresponding to values of $p \in P = \{0.8, 0.825, 0.85, 0.875, 0.9, 0.925, 0.95, 0.975, 0.985, 0.995\}$, for both wet and dry working data defined in Section 3. These sample values are given in Table 3 for each one of the probed spatial scales.

Note that simplification of the index $\lambda \cdot A$ to just λ in the notation of sample quantiles and sample moments, is indeed justified, firstly by the fact that the data sets for which the estimates are obtained, consist of spatially (and temporally) pooled data from all sampled subregions of the same spatial scale λ, thus reducing the need to keep track of the reference scale region A, of which $\lambda \cdot A$ is a geometrically similar subregion, and secondly by the fact that all the sampled subregions have the same geometric shape of square.

5.1 Tail-quantiles and moments of wet epoch durations

A summary of statistical information regarding simple linear regressions of $\ln\{q_\lambda(p)/q_1(p)\}$ on $\ln\lambda$ for each $p \in P$ is given in Table 4. Correlation coefficients are satisfactorily high, slopes are quite significant, and intercept terms are rather insignificant, as inferred from p-values of corresponding t-tests. A plausible conclusion from this set of regressions is that wet quantiles seem to fit to a scaling format $\ln\{Q_\lambda(p)/Q_1(p)\} = \Theta(p) \cdot \ln\lambda$ or equivalently

$$Q_\lambda(p) = \lambda^{\Theta(p)} \cdot Q_1(p) \qquad (11),$$

which differs from simple scaling of quantiles as expressed by (6) in that the scaling exponent is a non-constant function $\Theta(p)$ of the probability level p.

Equation (11) formulates a certain type of multiscaling (in contrast to simple scaling with a single fixed exponent) of tail-quantiles, which hereafter we shall refer to as *power-law type of multiscaling*. That is, for a given probability p the scaling factor between p-quantiles at two different spatial scales equals the dimensionless ratio λ of the smaller to larger scale, raised to the power $\Theta(p)$.

Furthermore, simple linear regressions of $\ln q_\lambda(p)$ on $\ln(1-p)$ for each of the probed scales λ yield further insight about possible structure of wet duration tail-quantiles. Table 5 summarizes information from these regressions. Correlation coefficients are quite close to -1, while on the basis of p-values of corresponding t-tests both slopes and intercepts are statistically significant. This information points to the strong possibility of a linear relationship

$$\ln Q_\lambda(p) = A(\lambda) \cdot \ln(1-p) + \ln B(\lambda) \qquad (12),$$

where the slope and the intercept are, in general, some functions of the spatial scale λ, denoted by $A(\lambda)$ and $\ln B(\lambda)$ respectively.

From a mathematical standpoint, a plausible choice of functions which satisfy both equations (11) and (12) is $\ln B(\lambda) = \alpha \cdot \ln\lambda + \beta$, $A(\lambda) = \gamma \cdot \ln\lambda + \delta$, $\Theta(p) = \gamma \cdot \ln(1-p) + \alpha$, and in that case elementary algebraic manipulation of (11) and (12) yields that

$$Q_\lambda^{(w)}(p) = e^{\alpha \cdot \ln\lambda + \beta} \cdot (1-p)^{\gamma \cdot \ln\lambda + \delta} \qquad (13).$$

In order to estimate the parameters involved in this scenario, we regress intercepts from Table 5 against $\ln\lambda$, and we obtain $\alpha = 0.3652, \beta = 0.8746$ both statistically significant, with correlation coefficient 0.951. Similarly, regression of slopes from Table 5 against $\ln\lambda$ yields also significant $\gamma = 0.0285$ and $\delta = -0.5006$, with correlation coefficient 0.8884. Finally, simple linear regression of the slopes of Table 4 against $\ln(1-p)$ yields indeed the very same estimates obtained for the α and γ parameters, both significant again, although with a lower correlation coefficient equal to 0.7318. Figure 8 depicts the fit of these three linear regression lines to the corresponding scatterplots of points.

Figure 9 depicts a graphical comparison between sample quantiles and predicted tail-quantiles under the scenario postulated by equation (13) with the above estimated parameters. The comparison is based partly on values of the correlation coefficient between sample and predicted quantiles at each separate scale as well as cumulatively for all scales combined, and partly on scedasticity of scatterplots around the drawn diagonal line through the origin. It is rather clear that except perhaps of the largest probed scale (120 Km scale of reference) where the correlation is 0.879, the proposed scenario describes quite satisfactorily the variability of wet duration tail-quantiles across a wide range of spatial scales.

If equation (13) holds true for tail-quantiles, that is for every $p \in (p_0, 1)$ given some p_0 close to 1 (e.g. $p_0 = 0.8$), then the corresponding tail-probabilities ought to satisfy the equation

$$P\left(W_\lambda > Q_\lambda^{(w)}(p)\right) = 1 - p = \left[e^{-(\alpha \cdot \ln\lambda + \beta)} \cdot Q_\lambda^{(w)}(p)\right]^{1/(\gamma \cdot \ln\lambda + \delta)}, \quad \text{as} \quad p \nearrow 1,$$

whence by substitution of $Q_{\lambda}^{(w)}(p)$ with $u > 0$ follows that

$$P(W_{\lambda} > u) = e^{-(\alpha \cdot \ln \lambda + \beta) \,/\, (\gamma \cdot \ln \lambda + \delta)} \cdot u^{1/(\gamma \cdot \ln \lambda + \delta)}, \quad \text{as} \quad u \nearrow +\infty \qquad (14).$$

Equation (14) shows that under the scenario postulated by (13), tail probabilities of wet duration are of *hyperbolic type*, provided that $\gamma \cdot \ln \lambda + \delta < 0$, which indeed holds true for the above estimated values of $\gamma = 0.0285$ and $\delta = -0.5006$, since $0 < \lambda \leq 1$. Furthermore, if (13) is true, then equation (4) implies that

$$M_{\lambda}^{(w)}(n) > \int_{p_0}^{1} \left[Q_{\lambda}^{(w)}(p) \right]^n dp = e^{n(\alpha \cdot \ln \lambda + \beta)} \cdot \int_{p_0}^{1} (1-p)^{n(\gamma \cdot \ln \lambda + \delta)} dp \qquad (15),$$

and the latter integral is finite iff $n < -(\gamma \cdot \ln \lambda + \delta)^{-1}$. Therefore, if (13) is true, then at a given scale $0 < \lambda \leq 1$ the probability distribution of wet duration W_{λ} does not possess finite moments of order $-(\gamma \cdot \ln \lambda + \delta)^{-1}$ or higher. However, we should note that $-(\gamma \cdot \ln \lambda + \delta)^{-1}$ is not necessarily a tight upper bound of order up to which moments exist, because moments of some order smaller than this bound may also not exist due to possible non-integrability of the lower tail of the distribution near zero.

Hereafter we shall use $-(\gamma \cdot \ln \lambda + \delta)^{-1}$ merely as a crude estimate of highest order up to which moments of wet duration may exist. These estimates of moment order bounds for the probed scales $\lambda \in \Lambda = \{1/60,\ 2/60,\ 4/60,\ 8/60,\ 15/60,\ 30/60,\ 1\}$ are respectively equal to 1.62,1.67,1.73,1.79,1.85,1.92,1.99. It is interesting to note that these bounds imply that in everyone of the probed scales second order moments do not exist, and therefore duration of wet epochs is likely to have infinite variance.

In order to probe further the possibility of scaling in terms of moments we first focus on moments of order $k \in \{0.25,\ 0.5,\ 0.75,\ 1,\ 1.25,\ 1.50\}$, which presumably exist in all the seven probed scales under the scenario postulated by (13). A summary of statistical information regarding simple linear regressions of $\ln \{m_{\lambda}(k)/m_1(k)\}$ on $\ln \lambda$ for each one of these values of k is given in Table 6. Correlation coefficients are again satisfactorily high, slopes $S(k)$ are quite significant, and intercept terms are rather insignificant, as inferred from p-values of corresponding t-tests. A plausible conclusion from this set of regressions is that wet quantiles seem to fit to a scaling format $\ln \{M_{\lambda}(k)/M_1(k)\} = S(k) \cdot \ln \lambda$ or equivalently

$$M_{\lambda}(k) = \lambda^{S(k)} \cdot M_1(k) \qquad (16).$$

Equation (16) points to a power-law type of multiscaling scenario for moments of wet duration, as much as (11) points to a power-law type of multiscaling scenario for tail-quantiles of wet duration, provided that the function $S(k)$ is a non-linear function of k.

Figure 10(A) depicts regression lines fitted to points $(\ln \lambda, \ln \{m_{\lambda}(k)/m_1(k)\})$ for each value of moment order $k \in \{0.25,\ 0.5,\ 0.75,\ 1,\ 1.25,\ 1.50\}$, and Figure 10(B) depicts the variation of the slopes of these fitted lines. At first glance, Figure 10(B) indicates the very strong indeed possibility of a linear structural function $S(k)$. According to equation (7), this possibility would point to a simple scaling scenario, provided that the structural function had no intercept

term, and in that case the slope of $S(k)$ ought to be the scaling exponent parameter. However, linear regression of slopes $S(k)$ against moment orders $k \in \{0.25, 0.5, 0.75, 1, 1.25, 1.50\}$ from Table 6, yields a statistically significant intercept of -0.0574 (t-test p-value 0.0045), along with a linear slope 0.2990, and a very high indeed correlation coefficient 0.9976. Moreover, attentive reading of Figure 10(B) shows that the structural function $S(k)$ may well be some non-linear convex function of k, and despite how subtle this convexity may be, it certainly points to a power law multiscaling scenario for moments that would rule out the possibility of multiscaling of wet durations according to a multiplicative cascade process as defined in subsection 2.2.2, because then the structural function ought to be concave instead of convex.

If one is not aware of the previous analysis regarding tail-quantiles, which imposes certain restrictions on existence of moments, then moments of arbitrarily high order may be assumed to exist. For example, moments of order $k \in \{1, 2, 3, 4, 5, 6\}$ are often arbitrarily assumed to exist, and based on them one may proceed to their scaling analysis ignoring any other structure such as that of quantiles. Following this rather ad hoc approach, we regressed linearly again $\ln\{m_\lambda(k)/m_1(k)\}$ versus $\ln\lambda$ for each value of $k \in \{1, 2, 3, 4, 5, 6\}$. Information regarding this set of regressions is also given in Table 6, supporting again the power-law type of multiscaling for wet duration moments, but in this case the non-linearity of the structural function $S(k)$ seems to be concave as shown in Figure 10(C). Nevertheless, linear regression of $S(k)$ against moment orders $k \in \{1, 2, 3, 4, 5, 6\}$, yields a fairly good fit with correlation coefficient 0.9425, slope 0.1215, and a statistically significant intercept 0.23 (t-test p-value 0.0519).

Based on the above scaling analysis of moments one may tend to deduce that, despite some non-linearity of the structural function, there is enough evidence to support scenaria of simple scaling, such as the one with scaling exponent $\theta = 0.2990$ obtained from moments of order $k \in \{0.25, 0.5, 0.75, 1, 1.25, 1.50\}$, or alternatively the one with scaling exponent $\theta = 0.1215$ obtained from moments of order $k \in \{1, 2, 3, 4, 5, 6\}$. In either case, tail-quantiles ought to also scale according to equation (6). Figure 11 depicts a graphical comparison between sample quantiles and predicted tail-quantiles under three different scenaria. These are, the power-law type of multiscaling scenario postulated by equation (13) with the above estimated parameters, and the two simple scaling scenaria with scaling exponents $\theta = 0.2990$ and $\theta = 0.1215$ respectively. As in Figure 9, the comparison is based partly on values of the correlation coefficient between sample and predicted quantiles, and partly on scedasticity of scatterplots around the drawn diagonal line through the origin. Plots in the left column of plots in Figure 11 combine sample and predicted tail-quantiles from all spatial scales, while plots in the right column combine sample and predicted tail-quantiles from all scales but the 120 Km scale of reference. Inclusion of the scale of reference clearly introduces some bias in favor of the simple scaling scenaria by contributing ten points (as many as the values of $p \in P$ for which tail-quantiles are obtained) displayed exactly along the diagonal of each scatterplot. Nevertheless, it is very clear that the power-law type of multiscaling scenario according to (13) describes the predicted variability of wet duration

tail-quantiles better than the simple scaling scenaria at all scales, both in terms of higher correlation with sample quantiles and in terms of better fit along the diagonal through the origin.

We believe that this last result is quite informative in many aspects when juxtaposed to the finding of Pavlopoulos and Gritsis (1999) that wet duration of regional rainfall is a simple scaling process with scaling exponent $\theta = 0.2537$. That result was obtained from scaling analysis of moments of order $k \in \{1, 2, 3, 4, 5\}$ from a much smaller section of TOGA-COARE data over a square region of size $10 \times 10\ Km^2$ during the entire Cruise 2 (December 20, 1992 through January 9, 1993) with temporal resolution 10 *minutes*. The very limited size of the region for which data was available for that study, limited also the scaling analysis to only five spatial scales (10 Km, 8 Km, 6 Km, 4 Km, and 2 Km), and was based only on an individual system of nested subregions at these scales since spatial pooling was clearly not much of an option.

In order to compare more closely the results of this study with the results of Pavlopoulos and Gritsis (1999) about spatial scaling of wet duration of regional rainfall, we made some extra effort to investigate scaling of the wet working data across the restricted range of scales corresponding to 16 Km, 8 Km, 4 Km, and 2 Km. The result is quite remarkable indeed, in that it literally reverts the previous conclusion in favor of simple scaling over these smaller scales. Specifically, working along the same line of regressions as for all scales, scaling analysis of moments of order $k \in \{0.25, 0.5, 0.75, 1, 1.25, 1.50\}$ and of order $k \in \{1, 2, 3, 4, 5, 6\}$ both point to validity of (16) again, with structural functions $S(k)$ deviating in a very subtle but clearly convex manner from linearity, with extremely high correlation coefficients (0.9996 and 0.9957 respectively), slopes 0.1492 and 0.2341 respectively, and statistically significant intercepts -0.0119 (t-test p-value 0.0048) and -0.1532 (t-test p-value 0.0221) respectively. Figure 12 serves the purpose of comparison between the power-law multiscaling scenario (13) for wet tail-quantiles against the two simple scaling scenaria with scaling exponents $\theta = 0.1492$ and $\theta = 0.2341$ respectively. Evidently, the competition between simple scaling and power-law multiscaling is much closer in terms of the fit of points along the diagonal, and simple scaling is slightly better in terms of correlation between predicted and sample tail-quantiles, a situation indeed opposite to the one over all scales as depicted in Figure 11.

5.2 Tail-quantiles and moments of dry epoch durations

Unlike tail-quantiles of wet duration, tail-quantiles of dry working data do not support the validity of equation (11). This is easily concluded from the statistical information obtained from linear regressions of $\ln\{q_\lambda(p)/q_1(p)\}$ on $\ln\lambda$ for each $p \in P$, which is very poor to support linearity. Instead, linear regressions of $\ln\{q_\lambda(p)/q_1(p)\}$ on the spatial scale λ itself, for each $p \in P$, yield quite strong evidence of linearity with extremely close to -1 correlation coefficients below -0.97, and statistically significant intercepts which apparently are opposite to values of the corresponding slopes. Further confirmation of this structure is obtained via linear regressions of $\ln\{q_\lambda(p)/q_1(p)\}$ on $\lambda - 1$ for each $p \in P$. Information from this latter set of regressions is given in Table 7, where

correlations and slopes remarkably match exactly those obtain from regressions of $\ln\{q_\lambda(p)/q_1(p)\}$ on λ, and intercepts are quite insignificant as we anticipated from inclusion of their significant part into the regressor $\lambda - 1$ by subtraction of unity. Thus, a plausible conclusion is that dry quantiles fit to a scaling format $\ln\{Q_\lambda(p)/Q_1(p)\} = \Psi(p) \cdot (\lambda - 1)$ or equivalently

$$Q_\lambda(p) = e^{\Psi(p)\cdot(\lambda-1)} \cdot Q_1(p) \qquad (17).$$

Equation (17) is clearly different from both simple scaling of quantiles formulated by (6) and power-law multiscaling of quantiles formulated by (11), and formulates a new type of multiscaling of tail-quantiles, which hereafter we shall refer to as *exponential type of multiscaling.* This nomenclature is justified by the fact that for a given probability p the scaling factor between p-quantiles at two different spatial scales is an *exponential function* of the dimensionless ratio λ of the smaller to larger scale, and the exponent of this scaling factor is a linear function of λ with slope $\Psi(p)$ and intercept $-\Psi(p)$ which are themselves *non-constant* functions of p.

Furthermore, simple linear regressions of $\ln q_\lambda(p)$ on $\ln(1-p)$ for each of the probed scales λ yield further useful insight about possible structure of dry duration tail-quantiles. Table 8 summarizes information from these regressions. Correlation coefficients are quite close to -1, while on the basis of p-values of corresponding t-tests both slopes and intercepts are statistically significant (except possibly of the intercept at the 16 Km and 30 Km scales). This information points anew to the strong possibility of a linear relationship

$$\ln Q_\lambda(p) = A^*(\lambda) \cdot \ln(1-p) + \ln B^*(\lambda) \qquad (18),$$

where the slope and the intercept are, in general, some functions of the spatial scale λ, denoted by $A^*(\lambda)$ and $\ln B^*(\lambda)$ respectively.

From a mathematical standpoint, equation (18) for dry tail-quantiles is of the same form as equation (12) for wet tail-quantiles, except that now a plausible set of functions which satisfy both (17) and (18) is $\ln B^*(\lambda) = \alpha^* \cdot \lambda + \beta^*$, $A^*(\lambda) = \gamma^* \cdot \lambda + \delta^*$, $\Psi(p) = \gamma^* \cdot \ln(1-p) + \alpha^*$, and in that case it follows easily from (17) and (18) that

$$Q_\lambda^{(d)}(p) = e^{\alpha^*\cdot\lambda+\beta^*} \cdot (1-p)^{\gamma^*\cdot\lambda+\delta^*} \qquad (19).$$

In order to estimate the parameters involved in this scenario, we regress intercepts from Table 8 against λ, and we obtain $\alpha^* = -0.5117$, $\beta^* = 0.2327$ both statistically significant, with negative correlation coefficient -0.7958. Similarly, regression of slopes from Table 8 against λ yields also significant $\gamma^* = 0.379$ and $\delta^* = -0.57$, with correlation coefficient 0.9415. Finally, simple linear regression of the slopes of Table 7 against $\ln(1-p)$ yields indeed the very same estimates obtained for the α^* and γ^* parameters, both significant again, with correlation coefficient 0.9792. Figure 13 depicts the fit of these three linear regression lines to the corresponding scatterplots of points, and Figure 14 depicts a graphical comparison between sample quantiles and predicted tail-quantiles under the scenario postulated by equation (19) with the above estimated parameters.

Clearly, the proposed scenario describes quite satisfactorily the variability of dry duration tail-quantiles across the probed spatial scales.

If (19) truly holds for dry tail-quantiles, then the corresponding tail-probabilities ought to satisfy the equation

$$P\left(D_\lambda > Q_\lambda^{(d)}(p)\right) = 1 - p = \left[e^{-(\alpha^* \cdot \lambda + \beta^*)} \cdot Q_\lambda^{(d)}(p)\right]^{1/(\gamma^* \cdot \lambda + \delta^*)}, \quad \text{as} \quad p \nearrow 1,$$

whence by substitution of $Q_\lambda^{(d)}(p)$ with $u > 0$ follows that

$$P\left(D_\lambda > u\right) = e^{-(\alpha^* \cdot \lambda + \beta^*) \,/\, (\gamma^* \cdot \lambda + \delta^*)} \cdot u^{1/(\gamma^* \cdot \lambda + \delta^*)}, \quad \text{as} \quad u \nearrow +\infty \qquad (20),$$

showing that under the scenario postulated by (19) tail probabilities of dry duration are also of *hyperbolic type*, provided that $\gamma^* \cdot \lambda + \delta^* < 0$, which indeed holds true for the obtained estimates of γ^* and δ^*. Furthermore, if (13) is true, then equation (4) implies that for p_0 in a neighborhood of 1,

$$M_\lambda^{(d)}(n) > \int_{p_0}^{1} \left[Q_\lambda^{(d)}(p)\right]^n dp = e^{n(\alpha^* \cdot \lambda + \beta^*)} \cdot \int_{p_0}^{1} (1-p)^{n(\gamma^* \cdot \lambda + \delta^*)} dp \qquad (21),$$

and the latter integral is finite iff $n < -(\gamma^* \cdot \lambda + \delta^*)^{-1}$ which can be used as a crude upper bound for the order of finite moments of dry duration at a given scale. These bounds for the probed scales $\lambda \in \Lambda$={1/60, 2/60, 4/60, 8/60, 15/60, 30/60, 1} are respectively equal to 1.77, 1.79, 1.83, 1.92, 2.10, 2.62, 5.23. It is interesting to note that according to these bounds, duration of dry epochs is likely to have infinite variance for scales of 16 Km or less.

In order to probe scaling in terms of moments of dry duration we consider sample moments of order $k \in$ {0.25, 0.5, 0.75, 1, 1.25, 1.50, 2, 3, 4, 5, 6}, and start with linear regressions of $\ln\{m_\lambda(k)/m_1(k)\}$ on $\ln\lambda$ for each value of k. Table 9 summarizes information from these regressions, where we note that for $k \in$ {0.25, 0.5, 0.75, 1, 1.25, 1.50}, so that the corresponding moments ought to probably exist in all scales under the scenario postulated by (10), correlation coefficients are moderately close to -1, whereas for $k \in$ {2, 3, 4, 5, 6} they begin to increase significantly and thus weakening the evidence of linearity. Moreover, intercept terms are rather significant as inferred from p-values of corresponding t-tests. These findings suggest that, unlike moments of wet duration, moments of dry duration probably do not conform with a power-law type of multiscaling $M_\lambda^{(d)}(k) = \lambda^{S^*(k)} \cdot M_1^{(d)}(k)$, and consequently neither to simple scaling.

Figure 15(A) depicts regression lines fitted to points $(\ln\lambda, \ln\{m_\lambda(k)/m_1(k)\})$ for each value of moment order $k \in$ {0.25, 0.5, 0.75, 1, 1.25, 1.50}, while Figures 15(B) and 15(C) depict the variation of the slopes $S^*(k)$ of two subsets of linear regressions corresponding to values of k in the sets {0.25, 0.5, 0.75, 1, 1.25, 1.50} and {1, 2, 3, 4, 5, 6} respectively. Despite a very slight concavity of the "pseudo-structural" function $S^*(k)$ indicated in both Figures 15(B) and 15(C), the most prominent impression is that $S^*(k)$ could very well be a linear function of k. Indeed, regression of the two sets of slopes $S^*(k)$ on the corresponding values of k, yield correlation coefficients -0.9944 and -0.9994 both pointing to very strong linearity, slopes -0.3292 and -0.5036 respectively, and statistically

significant intercepts 0.0593 (t-test p-value 0.0251) and 0.2962 (t-test p-value 0.0008) respectively. We note that the significance of the latter two intercepts can be interpreted as additional evidence against a simple scaling scenario, but if we want to test for (or against) such a scenario, then our first crude estimates of a possible "scaling exponent" would be θ = -0.3292 and θ = -0.5036.

Graphical comparisons between sample tail-quantiles and predicted tail-quantiles for dry duration, based on (6) for simple scaling with θ = -0.3292 and θ = -0.5036, and alternatively based on the exponential type of multiscaling scenario postulated by (19) with the above estimated parameters α^*, β^*, γ^*, δ^*, are depicted in Figure 16, whence very clearly the scenario of exponentially multiscaling describes the variability of dry duration tail-quantiles strikingly well, and by far better than either of the simple scaling scenaria, at all scales.

Having ruled out the possibility of power-law type of multiscaling for moments of dry duration, based on the above presented evidence, and guided by the hint that moments and tail-quantiles of wet duration conform to the same type of scaling (power-law multiscaling), we proceed to investigate if such "symmetry" holds also for dry durations. That is, we proceed to investigate exponential type of multiscaling for moments of dry duration as an alternative scenario. To this end, we regressed $\ln\{m_\lambda(k)/m_1(k)\}$ on $\lambda-1$ for each $k \in$\{0.25, 0.5, 0.75, 1, 1.25, 1.50, 2, 3, 4, 5, 6\}, and statistical information from these regressions is summarized in Table 10. Indeed, correlation coefficients point to an extremely strong linear relationship $\ln\{M_\lambda(k)/M_1(k)\} = H(k)\cdot(\lambda-1)$, with negative slope denoted by the function $H(k)$, and negligible (i.e. statistically insignificant) intercept. That is, the latter set of regressions yields ample evidence supportive of exponential multiscaling of dry moments according to the formula

$$M_\lambda(k) = e^{H(k)\cdot(\lambda-1)} \cdot M_1(k) \qquad (22),$$

which expresses exponential type multiscaling of dry duration moments, and notably can be viewed as a special case of (10) with

$$\Xi_\lambda(k) = e^{H(k)\cdot(\lambda-1)} \qquad (23).$$

Figure 17(A) depicts regression lines fitted to points $(\lambda-1, \ln\{m_\lambda(k)/m_1(k)\})$ for each value of moment order $k \in$\{0.25, 0.5, 0.75, 1, 1.25, 1.50\}, while Figures 17(B) and 17(C) depict the variation of the slopes $H(k)$ of two subsets of linear regressions corresponding to values of k in the sets {0.25, 0.5, 0.75, 1, 1.25, 1.50} and {1, 2, 3, 4, 5, 6} respectively. Despite a very slight concavity of the function $H(k)$ indicated in both Figures 17(B) and 17(C), the most prominent impression is that $H(k)$ could very well be a linear function of k as well. Indeed, regression of the two sets of slopes $H(k)$ on the corresponding values of k, yield correlation coefficients -0.9934 and -0.9989 both pointing to very strong linearity, slopes -1.5032 and -2.5011 respectively, and statistically significant intercepts 0.2863 (t-test p-value 0.0273) and 1.6871 (t-test p-value 0.0019) respectively.

It is interesting to remark that the second derivative $\Xi''_\lambda(k) = \Xi_\lambda(k)\cdot(\lambda-1)\cdot\left\{H''(k) + (\lambda-1)\cdot\left[H'(k)\right]^2\right\}$, of $\Xi_\lambda(k)$ in (23), with respect to k, has positive sign if $H(k)$ is non-linear concave function, and negative sign if $H(k)$ is

linear function. Consequently, if $H(k)$ is non-linear concave, then $\Xi_\lambda(k)$ is a convex function of k as in the multiscaling framework of multiplicative cascade processes where (10) is anticipated to hold true, and if $H(k)$ is linear, then $\Xi_\lambda(k)$ is a concave function of k.

Another "symmetry" (so to speak) which seems to hold between wet and dry durations of regional rainfall is that, if we restrict the scaling analysis of tail-quantiles and moments of dry durations to the narrower range of scales corresponding to 16 Km, 8 Km, 4 Km, and 2 Km, then although there is still ample evidence supporting quite firmly exponential multiscaling of both tail-quantiles and moments, we find that analysis of sample moments yields also substantial evidence of simple scaling scenaria. Specifically, analyses of moments of order $k \in \{0.25, 0.5, 0.75, 1, 1.25, 1.50\}$ and of order $k \in \{1, 2, 3, 4, 5, 6\}$, both point to structural functions deviating in a very subtle but clearly concave manner from linearity, with extremely strong correlation coefficients (-0.9959 and -0.9987 respectively), slopes -0.0885 and -0.1070 respectively, and statistically significant intercepts 0.0144 (t-test p-value 0.0212) and 0.0294 (t-test p-value 0.0476) respectively. Along with significance of these intercepts, another fact that weakens the possibility of simple scaling is also the significance of intercepts in regressions of $\ln\{m_\lambda(k)/m_1(k)\}$ versus $\ln\lambda$. However, using the latter two slopes as estimates of scaling exponents, Figure 18 serves the purpose of comparison over these lower scales, between sample and predicted tail-quantiles of dry durations under the exponential multiscaling scenario (19) and the two simple scaling scenaria with scaling exponents θ = -0.0885 and θ = -0.1070 respectively. It can be seen that although the fit of points along the diagonal line through the origin is better under the exponential multiscaling scenario, the two simple scaling scenaria yield slightly higher correlation coefficients (0.9974 and 0.9972) between sample and predicted tail-quantiles than the correlation coefficient 0.9861 obtained under exponential multiscaling, and clearly simple scaling is rendered here more competitive against exponential multiscaling than in the comparison made in Figure 16.

Closing this section we note that simple scaling of dry duration of regional rainfall was also reported among the results obtained by Pavlopoulos and Gritsis (1999), with quite different scaling exponent $\theta^{(d)}$ = -0.3360, based there on scaling analysis of sample moments of order $k \in \{1, 2, 3, 4, 5\}$ for the same individual system of nested subregions (corresponding to scales of 10 Km, 8 Km, 6 Km, 4 Km, and 2 Km) that pointed to simple scaling of wet duration with scaling exponent $\theta^{(w)} = 0.2537$.

5.3 Capacity fractal dimension of wet residence time

Hyperbolic tail-probabilities expressed by formulae (14) and (20), for wet and dry epoch durations respectively, besides leading to bounds of the order up to which moments may exist, also point to the fractal or multifractal nature of the set where wet epochs are supported in time records of regional rainfall. Such a set is hereafter referred to as *wet residence time* of regional rainfall, and in this subsection we are concerned with the dependence of fractal dimension of wet residence time on the spatial scale to which regional rainfall records correspond.

A general account on the connection between hyperbolic distributions and fractals is given by Mandelbrot (1983), but more specifically related to the approach undertaken here is the work by Schmitt *et al.* (1998), where it is shown that the probability density function of dry residence is proportional to $\tau^{-(\Delta+1)}$, where Δ is the fractal dimension of the wet residence set in a temporal record of rainfall, at given temporal scale τ, at a fixed site. This very result has also been obtained by Lowen and Teich (1993), although by an approach different than that of Schmitt *et al.* (1998).

In any event, the argument given by Schmitt *et al.* (1998), based on average number of dry epochs accounted at a given temporal scale τ, is also valid if the temporal record is a record of regional rainfall over a whole region of some scale, instead of a record at a single point location. Thus, in the more general regional setting, the probability density function of dry residence is also anticipated to be proportional to $\tau^{-(\Delta_\lambda+1)}$, where Δ_λ is now the fractal dimension of the wet residence set in a temporal record of *regional* rainfall, at given temporal scale τ, over a region of spatial scale λ. Consequently, integration with respect to τ, yields tail-probabilities of dry duration (or dry residence time) D_λ being proportional to $\tau^{-\Delta_\lambda}$. That is, $P(D_\lambda > \tau) \propto \tau^{-\Delta_\lambda}$, whence for $\tau = Q_\lambda^{(d)}(p)$ we obtain $1-p \propto \left[Q_\lambda^{(d)}(p)\right]^{-\Delta_\lambda}$, or equivalently $Q_\lambda^{(d)}(p) \propto (1-p)^{-1/\Delta_\lambda}$, and if $\sigma_\lambda > 0$ denotes the constant of proportionality in the latter relationship, then we have that

$$Q_\lambda^{(d)}(p) = \sigma_\lambda \cdot (1-p)^{-1/\Delta_\lambda} \qquad (24).$$

For $p \nearrow 1$, one may combine equation (19) for tail-quantiles with equation (24) to obtain

$$\frac{\sigma_\lambda}{\sigma_1} \cdot (1-p)^{-\frac{1}{\Delta_\lambda}+\frac{1}{\Delta_1}} = \frac{Q_\lambda^{(d)}(p)}{Q_1^{(d)}(p)} = e^{\alpha^* \cdot (\lambda-1)} \cdot (1-p)^{\gamma^* \cdot (\lambda-1)},$$

whence by solving for the exponent of $1-p$ on the LHS it follows that

$$\frac{1}{\Delta_\lambda} - \frac{1}{\Delta_1} = \gamma^* \cdot (1-\lambda) + \ln\left\{\sigma_\lambda \cdot e^{\alpha^* \cdot (1-\lambda)}/\sigma_1\right\} / \ln(1-p) \qquad (25).$$

Noting that the second term in the RHS of (25) tends to vanish as $p \nearrow 1$, we deduce that

$$\frac{1}{\Delta_\lambda} - \frac{1}{\Delta_1} = \gamma^* \cdot (1-\lambda) + o(\ln(1-p)) \qquad (26).$$

Equation (26) presents both theoretical and practical interest as it expresses a rather simple *approximate* linear relationship of the inverse fractal dimension $1/\Delta_\lambda$ of wet residence time of regional rainfall records, with respect to the spatial scale λ of the region. The slope is determined by the parameter γ^* of dry tail-quantiles (19), and the intercept is determined by the same parameter γ^* and also by the fractal dimension Δ_1 of wet residence time in regional rainfall records from a region at the spatial scale of reference, provided that all records are of the same temporal scale. Moreover, equation (26) readily implies that

fractal dimension of wet residence time decreases as spatial scale is reduced, pointing to *meagrening* of wet residence time as a region reduces in size.

In order to test equation (26), one first needs to obtain some estimates of the fractal dimensions on the LHS. To this end, we focused on the 155 time series records of spatially averaged rain rate from Cruise 1 only. Recall from Section 3 that these are 5 time series from sampled sub-regions at the scale of reference (120 Km), and 25 time series from sampled sub-regions at each one of the other six scales probed in this study. Cruise 1 (1992 scans) was preferred because it has nearly triple the number of scans than those available to us from Cruise 2 (617 scans). Concatenation of time series from Cruise 1 and Cruise 2 over any given sampled sub-region was not really an option, since there is a long gap of about eleven days between the end of Cruise 1 and the beginning of Cruise 2. However, the short blocks of missing scans within Cruise 1 were simply ignored, and an estimate of the *capacity fractal dimension* was obtained via a box-counting procedure for each one of these 155 time series (using unity as the embedding dimension of course). Some summary statistics of these estimates are given in Table 11, and Figure 19 depicts histograms of the distributions of box-counting estimates of the capacity fractal dimension in each scale. These are rather skewed histograms, suggesting that both the sample mean and the sample median may be used as gross estimates of the capacity fractal dimension Δ_λ at a given scale λ. Evidently, it is noticeable from the sample medians and from the sample means in Table 11, but also from the histograms in Figure 19, that as the spatial scale decreases there is a small but steady drift of probability mass towards smaller values of fractal dimension, as anticipated on the basis of (25) or (26).

Using the sample median of box-counting estimates as a gross estimate of the capacity dimension Δ_λ, for each scale λ, then simple linear regression of $1/\Delta_\lambda - 1/\Delta_1$ against $1 - \lambda$ yields correlation coefficient 0.8895, slope 0.5589, and a statistically negligible intercept -0.0652 (t-test p-value 0.5471), while using the sample means of box-counting estimates as gross estimates of capacity dimension in each scale, then linear regression of $1/\Delta_\lambda - 1/\Delta_1$ against $1 - \lambda$ yields correlation coefficient 0.9197, slope 0.5945, and also statistically negligible intercept -0.0699 (t-test p-value 0.4697).

Both these regressions show that although correlation coefficients are not strikingly high, they are significant enough to support linearity, while intercepts are statistically negligible as we anticipated according to (26). The only shortcoming of these regressions is that they yield slopes (0.5589 and 0.5945) which are higher than the estimated parameter $\gamma^* = 0.379$ from dry tail-quantiles. Nevertheless, scatterplots of points with coordinates $(0.379 \cdot (1 - \lambda), 1/\Delta_\lambda - 1/\Delta_1)$, marked in Figure 20 with $\Box$ for median and with $\divideontimes$ for mean gross estimates of capacity dimension, show that the predictor $0.379 \cdot (1 - \lambda)$ underestimates the difference $1/\Delta_\lambda - 1/\Delta_1$ only in the lower spectrum of spatial scales between 2 Km and 8 Km, and possibly up to 16 Km if the mean gross estimate of capacity dimension is used, while in the upper spectrum of scales between 120 Km and 30 Km, and possibly down to 16 Km if the median gross estimate of capacity dimension is used, the theoretically obtained predictor $0.379 \cdot (1 - \lambda)$ matches quite closely the difference $1/\Delta_\lambda - 1/\Delta_1$ along the diagonal line drawn

through the origin.

We believe that these minor discrepancies ought to be attributed to the rather crude sample box-counting estimates of capacity dimensions, which were obtained from quite short time series of nearly 2000 observations sampled every 20 minutes, when it is well known that reliable estimation of a fractal dimension requires much richer time series data. Emphatically we mention that Schmitt *et al.* (1998) obtained a box-counting estimate of capacity dimension equal to 0.55, for temporal scales between 10 minutes and 3.5 days, from a single time series record of 29 years (January 1, 1967 through December 31, 1995) with sampling frequency of 10 minutes at a single point location (Uccle, Belgium). For a brief summary account on estimation of capacity fractal dimension via box-counting procedures, we refer to subsection 3.3.6 of the review article by Isham (1993) and references therein.

6 Concluding remarks and some thoughts

The work presented in this article is an effort to study spatial scaling properties of wet and dry epoch durations based on time series records of spatially averaged rain rate data (i.e. regional rainfall). Several limitations were pointed out regarding the information available from the data towards this goal. Some of these limitations were partially alleviated by spatio-temporal pooling of relevant information via implementation of a fixed (i.e. non-random) and symmetric design for sampling sub-regions of certain spatial scales from the region probed with TOGA-COARE. This pooling strategy required certain conditions of spatio-temporal homogeneity to hold, so that the scaling analysis be meaningful. Some effort was made to test these conditions, which provided sufficient statistical evidence supportive of the validity of spatial and temporal homogeneity to reasonable extent. Despite implementation of the pooling strategy as a means to exploit as much as possible available information, some inescapable limitations restricted the analysis on (upper) tail-quantiles only, on existing statistical moments, and on rather poor estimates of capacity dimensions of wet residence (time-) sets. Summarizing our findings in a nutshell, the main conclusions are:

1. Tail-quantiles and moments of wet epochs in regional rainfall records conform to power-law type of multiscaling, according to (11) and (16) respectively.

2. Tail-quantiles and moments of dry epochs in regional rainfall records conform to exponential type of multiscaling, according to (17) and (22) respectively.

3. Wet and dry epochs have (upper) tail-probabilities of hyperbolic type, according to (14) and (20) respectively.

4. The reciprocal of capacity dimension of wet residence time in a time series record of regional rainfall may be approximated by a linear function of the spatial scale of the region, according to (26).

Speculating on the consequences of the above findings, regarding aspects related to spatial and temporal modelling of rainfields, we address the wide

class of multifractal cascade models known for their potential to accommodate some multiscaling properties of the underlying random field, be it one-, two-, or even multi-dimensional.

Tail-probabilities of wet epochs being of hyperbolic type immediately rules out the possibility that time series records of regional rainfall at any spatial and temporal scale may be modelled by a one-dimensional β-cascade model, the simplest indeed cascade model, because it is well known that then tail-probabilities of wet epochs should be exponentially decaying (see Schmitt *et al.*, 1998).

Regarding the spatial process of wet durations $\{W_A \ ; \ A \subseteq S\}$ we deduce that, if the structural function $S(k)$ in (16) is non-linear convex, then a two-dimensional (2D) multiplicative cascade model whose factorial generator $\left\{C_\lambda^{(w)} \ ; \ \lambda \in (0,1]\right\}$ is independent of $\{W_A \ ; \ A \subseteq S\}$ would be inappropriate, because then the structural function in (10) ought to be concave instead of convex. However, the possibility of $\{W_A \ ; \ A \subseteq S\}$ being modelled by a positive 2D cascade remains promising, provided that its factorial generator $\left\{C_\lambda^{(w)} \ ; \ \lambda \in (0,1]\right\}$ is stochastically dependent on $\{W_A \ ; \ A \subseteq S\}$. This scenario readily amounts to having a joint probability density function between any two random variables W_A and $C_\lambda^{(w)}$, supported exclusively on the positive quadrant, and such that (8), (13), and (16) hold simultaneously.

Regarding the spatial process of dry durations $\{D_A \ ; \ A \subseteq S\}$, it was pointed out in sub-section 5.2 that if the function $H(k)$ in (22) is non-linear concave, then $\Xi_\lambda(k)$ is convex, and if $H(k)$ is linear, then $\Xi_\lambda(k)$ is concave. Therefore, if $H(k)$ is non-linear concave, then the process $\{D_A \ ; \ A \subseteq S\}$ may be modelled by a two-dimensional (2D) multiplicative cascade with factorial generator $\left\{C_\lambda^{(d)} \ ; \ \lambda \in (0,1]\right\}$ independent of $\{D_A \ ; \ A \subseteq S\}$. In the more likely case though, where $H(k)$ is linear function, the process $\{D_A \ ; \ A \subseteq S\}$ may be modelled by a two-dimensional (2D) multiplicative cascade only if there is a generator process $\left\{C_\lambda^{(d)} \ ; \ \lambda \in (0,1]\right\}$ which stochastically depends on $\{D_A \ ; \ A \subseteq S\}$ in such a manner that the joint probability density function between any two random variables D_A and $C_\lambda^{(d)}$ is supported exclusively on the positive quadrant again, and (8), (19), and (22) hold simultaneously.

It is not the scope of this article to establish from the mathematical standpoint the existence of dependent cascade processes possessing the desired multiscaling properties outlined above. Yet, putting such matters on a wider conceptual perspective, we believe that stochastic scale-invariance is a particular form of stochastic dependence across a range of different scales, and if cascade processes hold any promise to adequately model stochastic scale-invariance then probably there exist appropriate ones expressing the types of multiscaling discovered in the present work.

Another direction along which some basic research may be pursued, is to study to what extent the above multiscaling properties of wet and dry durations of regional rainfall may be retrieved from analyses like the ones shown here, but applied on simulated time-evolving random fields with spatio-temporal intermittence between zero and positive values. Such random fields may of course

be obtained by dynamic 2D cascades whose generator (not to be confused with the factorial generator process, which in fact is a limit product of replicas of the generator) is a non-negative random function of time with intermittence between zero and positive values. An example of such a dynamic 2D cascade is given by Over (1995) and Over and Gupta (1996), where the generator is a random function alternating between zero and positive values according to a binary stationary Markov process multiplied with an independent diffusion process whose stationary distribution is lognormal. Of course, many other alternatives may be explored. For instance, one may consider a 2D dynamic cascade whose generator is a random function alternating between zero and positive values according to a fractal renewal process [Lowen and Teich (1993)], with its positive sections being marked according to a 1D universal multifractal model [Schertzer and Lovejoy (1987), Tessier *et al.* (1993)], or according to an appropriate diffusion process [Pavlopoulos and Kedem (1992)]. Yet another alternative is to consider as generator a random function alternating between zero and positive values according to a hysteresis effect between two coupled brownian motions with drift [Freidlin and Pavlopoulos (1997)], with its positive sections being marked according to a third diffusion process again.

In parallel, whatever the cascade generator may be, development of efficient statistical methodologies such as maximum likelihood estimation is of great need in order to make inferences about model parameters and their physical interpretation. Unfortunately, this need has fallen missproportionately short of progress compared to the development of various types of multifractal cascade processes suitable for this or that modelling application. However, as the mathematical theory of cascades broadens and deepens, advanced statistical methodology beyond simple method of moments type of remedies is strongly anticipated to emerge eventually.

The space-time approach proposed here for probing intermittence of rainfields has the potential to be generalized so as to facilitate: a) exploitation of more information from rainfield map series such as TOGA-COARE, and b) establishment of "links" between duration and intensity of regional rainfall, and between duration of regional rainfall and fractional wet area, that is another truly space-time type of connection. Such "links", as the well known optimal threshold linear relationship between regional rain rate and fractional wet area where rain rate exceeds a given threshold [Kedem and Pavlopoulos (1991)], may lead to new statistical methodologies for inferences based on space-time data of rainfields probed via remote sensing technology. The key step towards such generalization is to introduce the concept of intermittence between wet and dry states, with respect to positive and zero values of regional rain rate, or with respect to positive and zero values of fractional wet area (or fractional dry area = 1-fractional wet area), not on the original random field but on versions obtained from it by truncation or clipping at certain threshold levels of pixel rain rate values. Suggestively, one may refer to this generalized concept of intermittence as *η-threshold level intermittence,* where $\eta \geq 0$ is a given threshold level according to which pixel rain rate values are clipped or truncated. Clearly $\eta = 0$ corresponds to the case of intermittence with respect to the original rainfield without any clipping or truncation of pixel rain rate values. One may anticipate that

for small values of the threshold (say for $\eta \leq 1$ *mm/hr*), the proposed analysis will benefit from reduction of the number of pixels with noisy small positive values of "rain rate" that could very well be representing instrument error and not actual rainfall, but at the cost of prolonging dry epochs and shortening wet epochs, which in turn eventually has an impact on inferences regarding scaling of quantiles and moments of wet and dry durations of regional rainfall.

Last and certainly not of least interest, would be the investigation of possible connections between scaling properties of spatial processes of wet and dry duration of regional rainfall, and scaling properties of flood peaks (and drought lows) with respect to size of drainage basins spanned by large river networks. Relatively recent work [Gupta *et al.* (1994), Gupta and Dawdy (1995)] has shown that, while flood peaks generated by snowmelt conform with simple scaling theories, flood peaks attributed to rainfall are multiscaling in a manner such that, for large return periods, spatial variability of flood peaks decreases as spatial scale increases. This effect may be attributed partly to multiscaling of regional rainfall intensity, where variability indeed decreases as spatial scale increases, but partly (possibly) to multiscaling of regional wet and dry duration processes as well. In fact, one may intuitively argue that over large continental regions (not oceanic as in this study), where drainage areas are spanned by river networks of substantial size in a terrain of complex geomorphology interacting with the atmospheric organization of rainfall, and given the reduced variability of regional rain intensity in such a large scale, the more important source of flood peak variability could very well be the spatial variability in wet and dry duration processes.

Acknowledgments

This research was supported by a joint grant from NSF/NASA and also by the European grant ERB-FMRX-CT96-0095 of the EU-TMR Network on "Computational and Statistical Methods for Spatial Data Analysis". Sincere thanks are expressed to Dr. Brian Mapes for providing us with a section of the TOGA-COARE data set.

References

[1] Barndorff-Nielsen, O.E., Gupta, V.K., Perez-Abrew, V., and Waymire, E., Eds. (1998): *Stochastic Methods in Hydrology*, World Scientific.

[2] Bickel, P.J. and K.A. Doksum (1977): *Mathematical Statistics: Basic Ideas and Selected Topics*, Holden-Day, Inc.

[3] Foufoula-Georgiou, E. and Georgakakos, K. (1991): Recent advances in space-time precipitation modeling and forecasting, Ch. 3 in *Recent Advances in the Modeling of Hydrological Systems*, Bowles, D., O'Connell, E. (Eds.), Reidel Publications Co.

[4] Foufoula-Georgiou, E. and Krajewski, W. (1995): Recent advances in rainfall modelling, estimation, and forecasting, *IUGG*, U.S. National Report 1991-1994, *Review Geophysics*, 1125-1137.

[5] Foufoula-Georgiou, E. (1998): On scaling theories of space-time rainfall: Some recent results and open problems. In *Stochastic Methods in Hydrology*, Barndorff-Nielsen, O.E., Gupta, V.K., Perez-Abrew, V., and Waymire, E. (Eds.), World Scientific, pp. 25-72.

[6] Freidlin, M. and H. Pavlopoulos (1997): On a stochastic model for moisture budget in an Eulerian atmospheric column, *Environmetrics*, **8**, 425-440.

[7] Gupta, V.K. and D.R. Dawdy (1995): Physical interpretations of regional variations in the scaling exponents of flood quantiles. In *Scale Issues in Hydrological Modelling*, J.D. Kalma and M. Sivapalan (Eds.), Wiley, pp. 105-119.

[8] Gupta, V.K., O.J. Mesa, and D.R. Dawdy (1994): Multiscaling theory of flood peaks: Regional quantile analysis, *Water Resources Research*, **30**(12), 3405-3421.

[9] Gupta, V. and E.C. Waymire (1990): Multiscaling properties of spatial rainfall and river flow distributions, *Journal of Geophysical Research*, **95**, 1999-2009.

[10] Gupta, V.K. and E.C. Waymire (1993): A statistical analysis of mesoscale rainfall as a random cascade, *Journal of Applied Meteorology*, **32**, 251-267.

[11] Gupta, V.K. and Waymire, E.C. (1998): Some mathematical aspects of rainfall, landforms, and floods. In *Stochastic Methods in Hydrology*, Barndorff-Nielsen, O.E., Gupta, V.K., Perez-Abrew, V., and Waymire, E. (Eds.), World Scientific, pp. 129-171.

[12] Harris, D. (1997): *Multiscaling Properties of Rainfall: Methods and Interpretation*, Ph. D. Dissertation, University of Auckland, Australia.

[13] Holley and E. Waymire (1992): Multifractal dimensions and scaling exponents for strongly bounded random cascades, *Annals of Applied Probability*, **2**, 819-845.

[14] Isham, V. (1993): Statistical aspects of chaos: A review. Ch. 3 in *Networks and Chaos: Statistical and Probabilistic Aspects*, Barndorff-Nielsen, O.E., Jensen, J.L., and Kendall, W.S. (Eds.), Chapman & Hall, pp. 124-200.

[15] Kalma, J.D and M. Sivapalan, Eds. (1995): *Scale Issues in Hydrological Modelling*, Wiley.

[16] Karr, A.F. (1993): *Probability*, Springer-Verlag.

[17] Kedem, B. and L.S. Chiu (1987): Are rain rate processes self similar?, *Water Resources Research*, **23**, 1816-1818.

[18] Kedem, B. and H. Pavlopoulos (1991): On the threshold method for rainfall estimation: Choosing the optimal threshold level, *Journal of the American Statistical Association*, **86**, 626-633.

[19] Lamperti, J. (1962): Semi-stable stochastic Processes, *Transactions of the American Mathematical Society*, **104**, 62-78.

[20] Lehmann, E.L. (1986): *Testing Statistical Hypotheses*, Second Edition, Wiley.

[21] Lovejoy, S. and B.B. Mandelbrot (1985): Fractal properties of rain and a fractal model, *Tellus*, **37A**, 209-232.

[22] Lovejoy, S. and D. Schertzer (1985): Generalized scale-invariance in the atmosphere and fractal models of rain, *Water Resources Research*, **21**(8), 1233-1250.

[23] Lowen, S.B. and M.C. Teich (1993): Fractal renewal processes generate 1/f noise, *Physical Review E*, **47**, 992-1001.

[24] Mandelbrot, B.B. (1983): *The Fractal Geometry of Nature*, W.H. Freeman & Co.

[25] Over, T. (1995): *Modeling Space-Time Rainfall at the Mesoscale Using Random Cascades*, Ph.D. Dissertation, University of Colorado at Boulder, USA.

[26] Over, T. and Gupta, V.K. (1996): A space-time theory of mesoscale rainfall using random cascades, *Journal of Geophysical Research*, **101**, 26319-26331.

[27] Pavlopoulos, H. and J. Gritsis (1999): Wet and dry epoch durations of spatially averaged rain rate, their probability distributions and scaling properties, *Environmental and Ecological Statistics*, **6**, 351-380.

[28] Pavlopoulos, H. and B. Kedem (1992): Stochastic modeling of rain rate processes: a diffusion model, *Stochastic Models*, **8**, 397-420.

[29] Pavlopoulos, H. and G. Makatis (1998): Spectral multiscaling of spatially averaged rain rate: a hint for spatio-temporal modeling, *Environmetrics*, **9**, 689-713.

[30] Rao, C.R. (1973): *Linear Statistical Inference and Its Applications*, Second Edition, Wiley.

[31] Rodriguez-Iturbe, I., M. Marani, P.D. Odorico, and A. Rinaldo (1998): On space-time scaling of cumulated rainfall fields, *Water Resources Research*, **34**(12), 3461-3469.

[32] Rohatgi, V.K. (1976): *An Introduction to Probability Theory and Mathematical Statistics*, Wiley.

[33] Schertzer, D. and S. Lovejoy (1987): Physical modeling and analysis of rain and clouds by anisotropic scaling multiplicative processes, *Journal of Geophysical Research*, **92**(D8), 9693-9714.

[34] Schmitt, F., S. Svannistsem, and A. Barbosa (1998): Modeling of rainfall time series using two-state renewal processes and multifractals, *Journal of Geophysical Research*, **103**(D18), 181-194.

[35] Short, D.A., Kucera, P.A., Ferrier, B.S., Gerlach, J. C., Rutledge, S. A. and Thiele, O.W. (1997): Shipboard radar rainfall patterns within the TOGA/COARE IFA, *Bulletin of the American Meteorological Society*, **78**, 2817-2836.

[36] Sposito, G., Editor (1998): *Scale Dependence and Scale Invariance in Hydrology*, Cambridge Univ. Press.

[37] Tessier, Y., S. Lovejoy, and D. Schertzer (1993): Universal multifractals: theory and observations for rain and clouds, *Journal of Applied Meteorology*, **32**, 223-250.

[38] Venugopal, V., E. Foufoula-Georgiou, and V. Sapozhnikov (1999): Evidence of dynamic scaling in space-time rainfall, *Journal of Geophysical Research*, **104**(D24), 599-610.

[39] Waymire, E. (1985): Scaling limits and self-similarity in precipitation fields, *Water Resources Research*, **21**(8), 1271-1281.

Table 1: Sample quantiles, in units of 20 minute intervals, at ten regularly spaced probability levels along each column, corresponding to spatio-temporally pooled working data of dry and wet spell lengths for each of the seven spatial scales.

DRY	120 Km	60 Km	30 Km	16 Km	8 Km	4 Km	2 Km	WET	120 Km	60 Km	30 Km	16 Km	8 Km	4 Km	2 Km
0.05	1	1	1	1	1	1	1	**0.05**	1	1	1	1	1	1	1
0.15	1	1	1	1	1	1	1	**0.15**	1	1	1	1	1	1	1
0.25	1	1	1	1	1	1	1	**0.25**	1	1	1	1	1	1	1
0.35	1	1	1	2	2	2	2	**0.35**	1	2	1	1	1	1	1
0.45	1	1	2	2	2	2	2	**0.45**	1	2	2	2	2	2	2
0.55	2	2	2	3	3	3	3	**0.55**	2	3	3	3	2	2	2
0.65	2	3	3	4	4	5	4	**0.65**	2.6	5	4	4	3	3	3
0.75	3	4	4	6	6	7	6	**0.75**	4	10	6	5	4	4	4
0.85	3.4	6	7	9	10	11	11	**0.85**	19.2	18	11	8	7	6	6
0.95	4	11	15	19.7	21	22	23	**0.95**	44.2	38	23	16	15	14	12

Table 3: Sample tail-quantiles of spatio-temporally pooled working data of dry and wet spell lengths for each of the seven spatial scales probed, at ten probability levels along each column. These estimates correspond to units of 20-minutes time length, which are converted to units of 1 hour (via multiplication by 1/3) when used for the scaling analysis.

DRY	120 Km	60 Km	30 Km	16 Km	8 Km	4 Km	2 Km	WET	120 Km	60 Km	30 Km	16 Km	8 Km	4 Km	2 Km
0.8	3	4	6	7	8	8	8	**0.8**	9.6	13	8	6	5	5	4
0.825	3	5	6	8	9	10	10	**0.825**	14.4	15	9	7	6	6	5
0.85	3.4	6	7	9	10	11	11	**0.85**	19.2	18	11	8	7	6	6
0.875	4	6	8	11	12	12	13	**0.875**	24	21	13	10	8	7	7
0.9	4	7.2	10	12	14	14	15	**0.9**	27	23	16	11	10	9	8
0.925	4	9	12	16	17	17	18	**0.925**	32.8	29	18	13	12	11	10
0.95	4	11	15	19.7	21	22	23	**0.95**	44.2	38	23	16	15	14	12
0.975	4	14	21	26	29	32	32	**0.975**	57.2	53	31	24	23.45	23	21
0.985	4.68	17	27	34	36	38.74	38	**0.985**	62.72	60.4	38	31	32	30	26
0.995	5.56	24.61	33.56	49.28	52.06	59.91	62.06	**0.995**	68.24	83.4	63.44	52	48.18	40.52	34

Table 2: P-values of tests of independence and of tests of homogeneity, between samples of wet spell lengths, and also between samples of dry spell lengths, for each pair of sub-regions of the same spatial scale sampled according to the NW-CR and NE-CR designs.

P-values of pairwise tests between NW-CR and NE-CR samples of WET spell lengths							
Spatial Scale	Independence Tests			Homogeneity Tests			
	$\chi 2$	Kendall	Spearman	$\chi 2$	Kolm-Sm	Wilcoxon	Kruskal
120 *Km*	0.9056	0.9990	0.9811	0.0287	0.1152	0.1544	0.1438
60 *Km*	0.1270	0.5511	0.4555	0.4647	0.8477	0.3731	0.3721
30 *Km*	0.4173	0.1758	0.1650	0.4757	0.7391	0.6962	0.6956
16 *Km*	0.1746	0.7169	0.7162	0.2516	0.5336	0.2216	0.2214
8 *Km*	0.8042	0.4031	0.3609	0.6017	0.9948	0.6358	0.6354
4 *Km*	0.5421	0.3429	0.3022	0.6771	0.9958	0.9207	0.9200
2 *Km*	0.1803	0.0532	0.0327	0.2806	0.5427	0.5735	0.5727
P-values of pairwise tests between NW-CR and NE-CR samples of DRY spell lengths							
Spatial Scale	Independence Tests			Homogeneity Tests			
	$\chi 2$	Kendall	Spearman	$\chi 2$	Kolm-Sm	Wilcoxon	Kruskal
120 *Km*	0.8643	0.1447	0.1090	0.4155	0.8524	0.3771	0.3689
60 *Km*	0.6076	0.6434	0.5888	0.9152	0.6742	0.4546	0.4538
30 *Km*	0.1895	0.4149	0.3661	0.3214	0.8149	0.2928	0.2925
16 *Km*	0.1372	0.4037	0.3798	0.9180	0.9991	0.9383	0.9378
8 *Km*	0.0735	0.1576	0.1536	0.4113	0.6377	0.3780	0.3776
4 *Km*	0.2370	0.2086	0.1827	0.7085	0.8135	0.5690	0.5682
2 *Km*	0.5530	0.5692	0.5353	0.6452	0.6066	0.3367	0.3360

Table 4: Summary statistics from the set of linear regressions of $\ln\{q_\lambda^{(w)}(p)/q_1^{(w)}(p)\}$ versus $\ln\lambda$, for each of the tail probability levels p. P-values from t-tests of significance (difference from zero) for the slope and intercept of each regression accompany in parentheses.

Probability Level p	Correlation Coefficient	Regression Slope $\Theta(p)$	Regression Intercept	Residual's Standard Error
0.8	0.9212	0.2625 (0.0032)	0.1749 (0.2096)	0.1781
0.825	0.9496	0.2839 (0.0010)	0.0143 (0.8947)	0.1507
0.85	0.9551	0.3220 (0.0008)	-0.0325 (0.7780)	0.1605
0.875	0.9627	0.3347 (0.0005)	-0.0568 (0.6052)	0.1512
0.9	0.9685	0.3145 (0.0003)	-0.0560 (0.5554)	0.1301
0.925	0.9523	0.3099 (0.0009)	-0.0718 (0.5386)	0.1597
0.95	0.9520	0.3323 (0.0009)	-0.0860 (0.4963)	0.1718
0.975	0.9133	0.2598 (0.0040)	-0.0923 (0.5001)	0.1863
0.985	0.9261	0.2211 (0.0027)	-0.0533 (0.6127)	0.1447
0.995	0.9442	0.2000 (0.0013)	0.1642 (0.0848)	0.1122

Table 5: Summary statistics from the set of linear regressions of $\ln q_\lambda^{(w)}(p)$ versus $\ln(1-p)$, for each of the probed spatial scales. P-values from t-tests of significance (difference from zero) for the slope and intercept of each regression accompany in parentheses.

Spatial Scale λ	Correlation Coefficient	Regression Slope $A(\lambda)$	Regression Intercept $\ln B(\lambda)$	Residual's Standard Error
1/60 (2Km)	-0.9782	-0.5865 (9×10^{-7})	-0.4216 (0.1410)	0.1598
2/60 (4 Km)	-0.9852	-0.5990 (2×10^{-7})	-0.3389 (0.0169)	0.1336
4/60 (8 Km)	-0.9894	-0.6153 (5×10^{-8})	-0.3047 (0.0143)	0.1158
8/60 (16 Km)	-0.9933	-0.5708 (8×10^{-9})	-0.0781 (0.3084)	0.0851
15/60 (30 Km)	-0.9858	-0.5424 (1×10^{-7})	0.2865 (0.0210)	0.1185
30/60 (60 Km)	-0.9764	-0.5069 (1×10^{-6})	0.8456 (0.0001)	0.1439
60/60 (120 Km)	-0.9028	-0.4906 (3×10^{-4})	0.9122 (0.0069)	0.2999

Table 6: Summary statistics from the set of linear regressions of $\ln\{m_\lambda^{(w)}(k)/m_1^{(w)}(k)\}$ versus $\ln\lambda$, for each value of moment order $k \in \{0.25, 0.5, 0.75, 1, 1.25, 1.5, 2, 3, 4, 5, 6\}$. P-values from t-tests of significance (difference from zero) for the slope and intercept of each regression accompany in parentheses.

Moment Order k	Correlation Coefficient	Regression Slope S(k)	Regression Intercept	Residual's Standard Error
0.25	0.9027	0.0314 (0.0053)	0.0328 (0.1025)	0.0241
0.5	0.9513	0.0839 (0.0009)	0.0414 (0.2233)	0.0437
0.75	0.9660	0.1554 (0.0004)	0.0224 (0.6435)	0.0668
1	0.9676	0.2374 (0.0003)	-0.0147 (0.8371)	0.0996
1.25	0.9661	0.3201 (0.0003)	-0.0568 (0.5710)	0.1375
1.5	0.9649	0.3965 (0.0004)	-0.0947 (0.4601)	0.1736
2	0.9651	0.5215 (0.0004)	-0.1433 (0.3982)	0.2275
3	0.9715	0.6812 (0.0002)	-0.1252 (0.5230)	0.2674
4	0.9701	0.7750 (0.0002)	0.0065 (0.9765)	0.3115
5	0.9498	0.8360 (0.0010)	0.2066 (0.5244)	0.4426
6	0.9109	0.8807 (0.0043)	0.4495 (0.3516)	0.6415

Table 7: Summary statistics from the set of linear regressions of $\ln\{q_\lambda^{(d)}(p)/q_1^{(d)}(p)\}$ versus $\lambda - 1$, for each of the tail probability levels p. P-values from t-tests of significance (difference from zero) for the slope and intercept of each regression accompany in parentheses.

Probability Level p	Correlation Coefficient	Regression Slope $\Psi(p)$	Regression Intercept	Residual's Standard Error
0.8	-0.9780	-1.0703 (1×10^{-4})	-0.0830 (0.3487)	0.0892
0.825	-0.9815	-1.2203 (8×10^{-5})	-0.0586 (0.5150)	0.0930
0.85	-0.9884	-1.1781 (2×10^{-5})	-0.0286 (0.6716)	0.0706
0.875	-0.9794	-1.2123 (1×10^{-4})	-0.0822 (0.3931)	0.0977
0.9	-0.9964	-1.3343 (1×10^{-6})	-0.0345 (0.4287)	0.0446
0.925	-0.9974	-1.5215 (6×10^{-7})	0.0122 (0.7630)	0.0428
0.95	-0.9969	-1.7490 (9×10^{-7})	0.0420 (0.4230)	0.0536
0.975	-0.9958	-2.0848 (2×10^{-6})	0.0712 (0.3395)	0.0749
0.985	-0.9938	-2.1344 (5×10^{-6})	0.0859 (0.3532)	0.0933
0.995	-0.9927	-2.3761 (8×10^{-6})	0.0876 (0.4284)	0.1130

Table 8: Summary statistics from the set of linear regressions of $\ln q_{\lambda}^{(d)}(p)$ versus $\ln(1-p)$, for each of the probed spatial scales. P-values from t-tests of significance (difference from zero) for the slope and intercept of each regression accompany in parentheses.

Spatial Scale λ	Correlation Coefficient	Regression Slope $A^*(\lambda)$	Regression Intercept $\ln B^*(\lambda)$	Residual's Standard Error
1/60 (2Km)	-0.9882	-0.5342 (8×10^{-8})	0.3149 (0.0078)	0.1060
2/60 (4 Km)	-0.9908	-0.5376 (3×10^{-8})	0.2785 (0.0081)	0.0943
4/60 (8 Km)	-0.9865	-0.5125 (1×10^{-7})	0.2938 (0.0127)	0.1090
8/60 (16 Km)	-0.9851	-0.5309 (2×10^{-7})	0.1472 (0.1807)	0.1189
15/60 (30 Km)	-0.9784	-0.5062 (9×10^{-7})	-0.0406 (0.7344)	0.1371
30/60 (60 Km)	-0.9807	-0.4704 (5×10^{-7})	-0.2524 (0.0377)	0.1203
60/60 (120 Km)	-0.9009	-0.1401 (3×10^{-4})	-0.1355 (0.1009)	0.0866

Table 9: Summary statistics from the set of linear regressions of $\ln\{m_{\lambda}^{(d)}(k)/m_{1}^{(d)}(k)\}$ versus $\ln\lambda$, for each value of moment order $k \in \{0.25, 0.5, 0.75, 1, 1.25, 1.5, 2, 3, 4, 5, 6\}$. P-values from t-tests of significance (difference from zero) for the slope and intercept of each regression accompany in parentheses.

Moment Order k	Correlation Coefficient	Regression Slope $S^*(k)$	Regression Intercept	Residual's Standard Error
0.25	-0.9260	-0.0436 (0.0027)	0.0359 (0.1246)	0.0285
0.5	-0.9222	-0.1004 (0.0031)	0.0884 (0.1138)	0.0676
0.75	-0.9177	-0.1710 (0.0035)	0.1605 (0.1049)	0.1190
1	-0.9125	-0.2545 (0.0041)	0.2544 (0.0977)	0.1834
1.25	-0.9069	-0.3494 (0.0048)	0.3705 (0.0920)	0.2610
1.5	-0.9009	-0.4535 (0.0056)	0.5078 (0.0875)	0.3511
2	-0.8894	-0.6817 (0.0073)	0.8370 (0.0812)	0.5630
3	-0.8698	-1.1823 (0.0109)	0.6512 (0.0747)	1.0779
4	-0.8539	-1.7046 (0.0144)	0.5976 (0.0716)	1.6702
5	-0.8403	-2.2285 (0.0179)	0.6261 (0.0698)	2.3109
6	-0.8289	-2.7476 (0.0211)	0.7035 (0.0686)	2.9806

Table 10: Summary statistics from the set of linear regressions of $\ln\{m_\lambda^{(d)}(k)/m_1^{(d)}(k)\}$ versus $\lambda - 1$, for each value of moment order $k \in \{0.25, 0.5, 0.75, 1, 1.25, 1.5, 2, 3, 4, 5, 6\}$. P-values from t-tests of significance (difference from zero) for the slope and intercept of each regression accompany in parentheses.

Moment Order k	Correlation Coefficient	Regression Slope H(k)	Regression Intercept	Residual's Standard Error
0.25	-0.9852	-0.1907 (5×10^{-5})	-0.0112 (0.3810)	0.0129
0.5	-0.9884	-0.4425 (2×10^{-5})	-0.0225 (0.3906)	0.0266
0.75	-0.9913	-0.7593 (1×10^{-5})	-0.0325 (0.4013)	0.0394
1	-0.9938	-1.1398 (5×10^{-6})	-0.0397 (0.4154)	0.0497
1.25	-0.9959	-1.5777 (2×10^{-6})	-0.0425 (0.4374)	0.0560
1.5	-0.9974	-2.0642 (6×10^{-7})	-0.0401 (0.4768)	0.0579
2	-0.9990	-3.1478 (5×10^{-8})	-0.0188 (0.7145)	0.0542
3	-0.9987	-5.5807 (9×10^{-8})	0.0799 (0.4476)	0.1078
4	-0.9968	-8.1804 (1×10^{-6})	0.2363 (0.3530)	0.2566
5	-0.9943	-10.8394(4×10^{-6})	0.4355 (0.3362)	0.4550
6	-0.9917	-13.5129(1×10^{-5})	0.6636 (0.3312)	0.6855

Table 11: Summary descriptive statistics of samples of box-counting estimates of capacity fractal dimension of wet residence sets for each one of the probed spatial scales. Fractal dimension estimates are based on TOGA-COARE, Cruise 1 time series of spatially averaged rain rate over sub-regions sampled according to the spatial sampling design described in Chapter 3.

Spatial Scale λ	Sample Median Capacity Dimension	Sample Mean Capacity Dimension	Sample Standard Deviation
1/60 (2Km)	0.5320	0.5277	0.0857
2/60 (4 Km)	0.5965	0.5717	0.1321
4/60 (8 Km)	0.5900	0.5776	0.0711
8/60 (16 Km)	0.6520	0.6037	0.1460
15/60 (30 Km)	0.6850	0.6757	0.0591
30/60 (60 Km)	0.7320	0.7191	0.0575
60/60 (120 Km)	0.8250	0.8088	0.0712

Figure 1: Instantaneous rain rate field retrieved from a typical radar scan over the region of study.

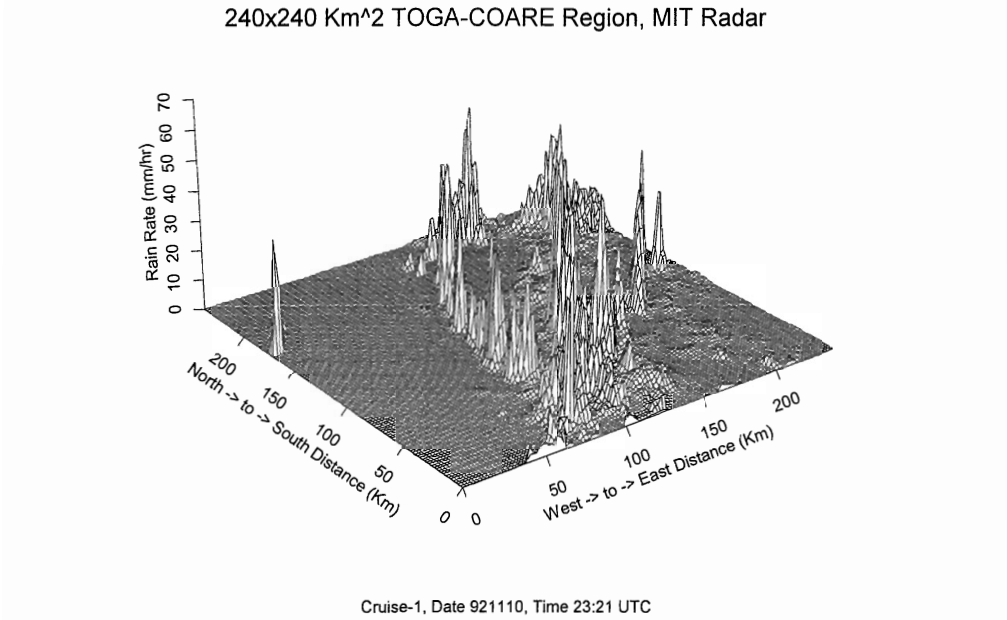

Figure 2: Spatial sampling design of five square sub-regions (NW, NE, SW, SE, CR), at the scale of reference (120 *Km* or $\lambda = 1$), from the TOGA-COARE 240x240 Km^2 square region of study.

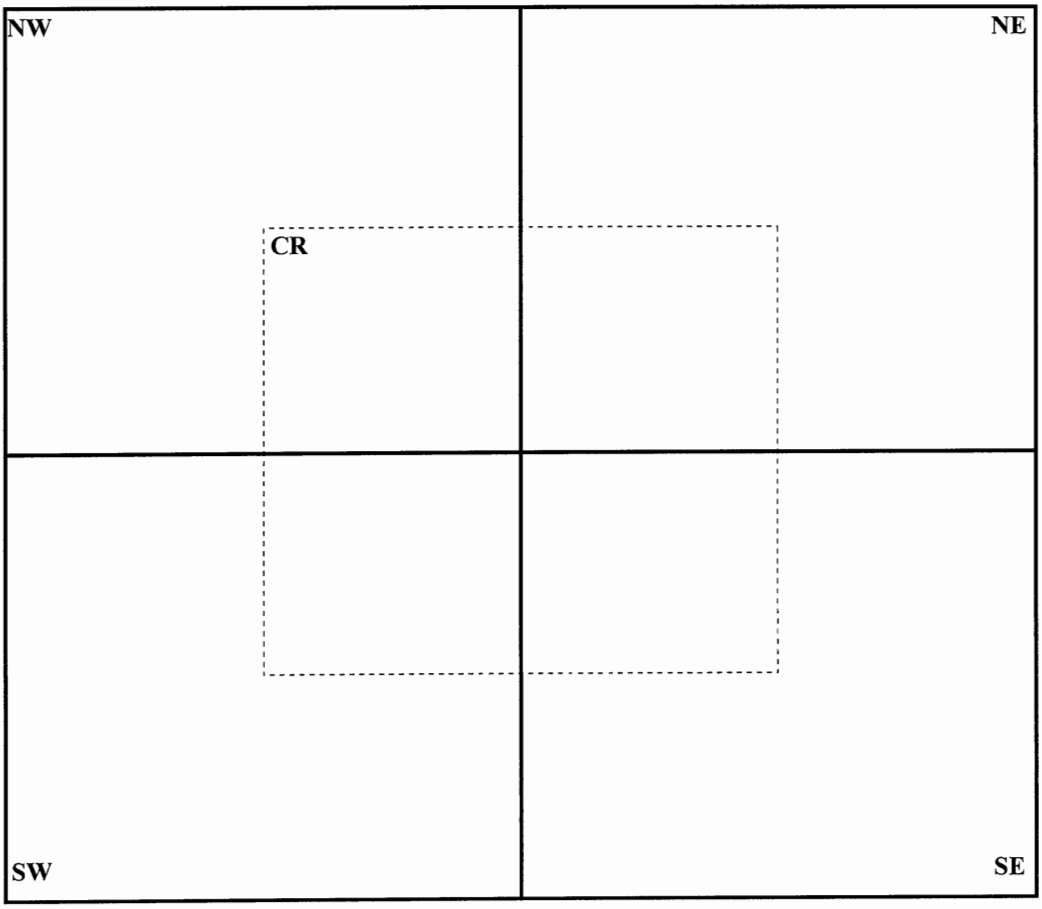

Figure 3: Five designs for spatial sampling of systems of six nested square sub-regions, corresponding to six spatial scales $\lambda \in \{60/120, 30/120, 16/120, 8/120, 4/120, 2/120\}$, from each one of the five square sub-regions of the reference scale ($\lambda = 120/120=1$) depicted in Figure 1. The dots imply the non-depicted smaller scales (1/120 for NW, NE, SW, SE, and 4/120, 2/120 for CR).

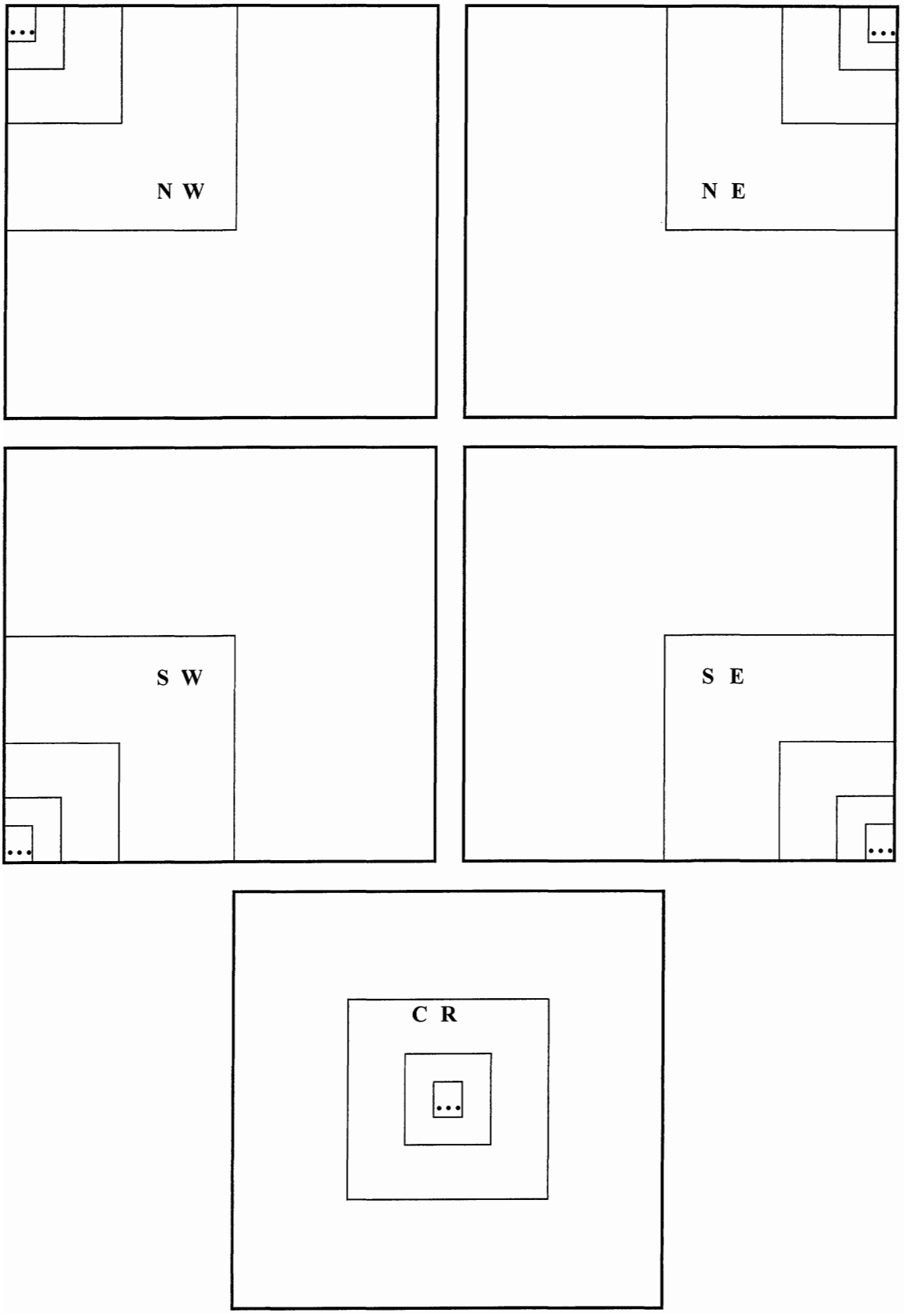

Figure 4: Time series of spatially averaged rain rate over the seven nested sub-regions sampled by the NE-CR design, during Cruise-1 (10 November through 9 December, 1992) of TOGA-COARE (MIT Radar). Sample sizes of dry and wet spells are also marked for each time series (e.g. the 60 Km NE-CR sub-region yields 88 dry spells and 75 wet spells), after discounting spells of ambiguous length due to missing values. Discounted spells are depicted as unit-gaps in each time series, modifying its length from 1992 to 2040.

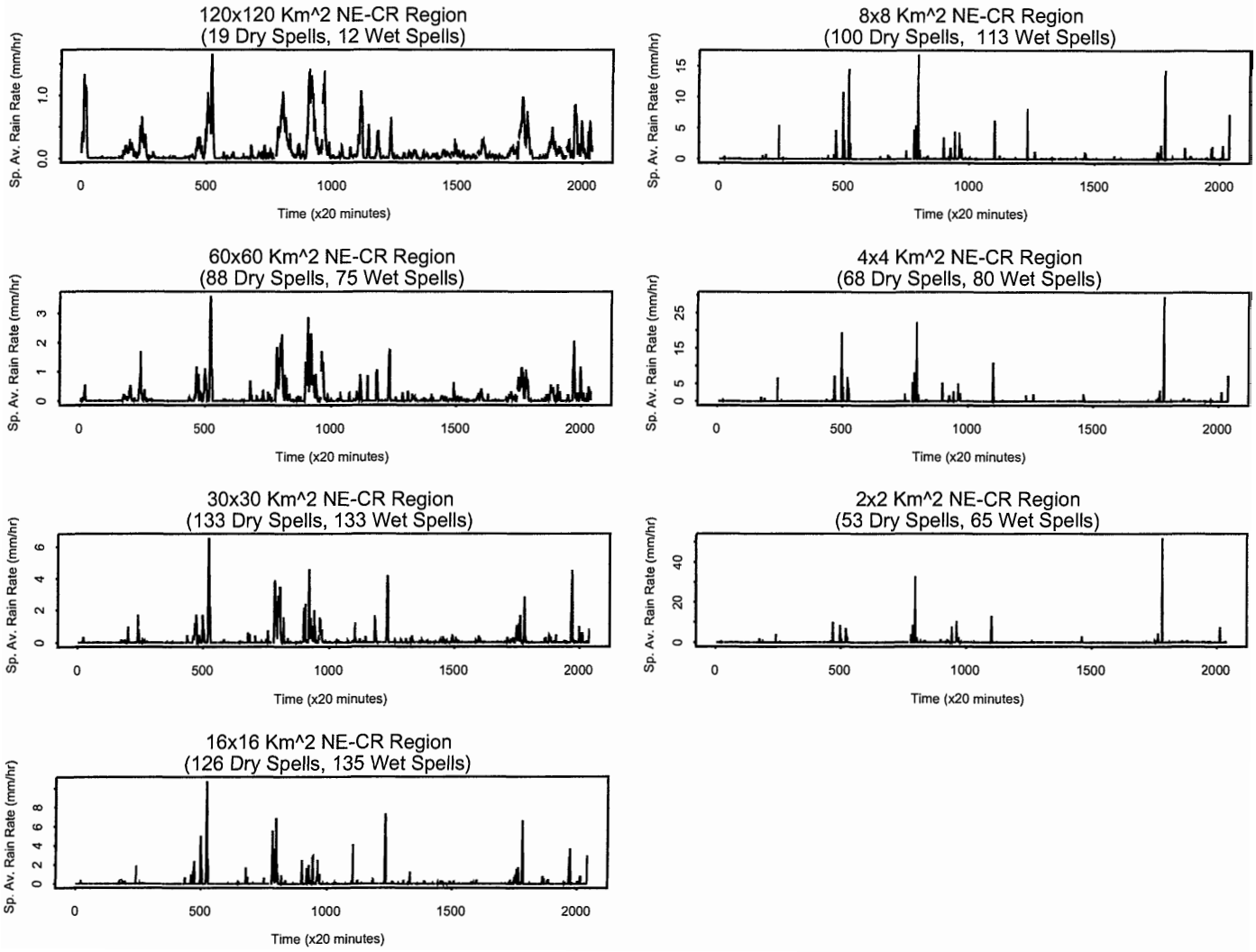

Figure 5: Box-plot summary statistics of dry (top row) and wet (bottom row) spell lengths sampled over the seven individual nested square sub-regions defined by the NE-CR design. Each vertical pair of box-plots corresponds to the same individual sub-region of the NE-CR design. Sample sizes of data are denoted by N under each box-plot (compare with sample sizes given in Figure 4). The upper and lower sides of each box indicate upper and lower quartiles, the white line inside each box indicates the median or middle quartile, and lines outside each box indicate extreme values in the upper tail of the underlying probability distribution.

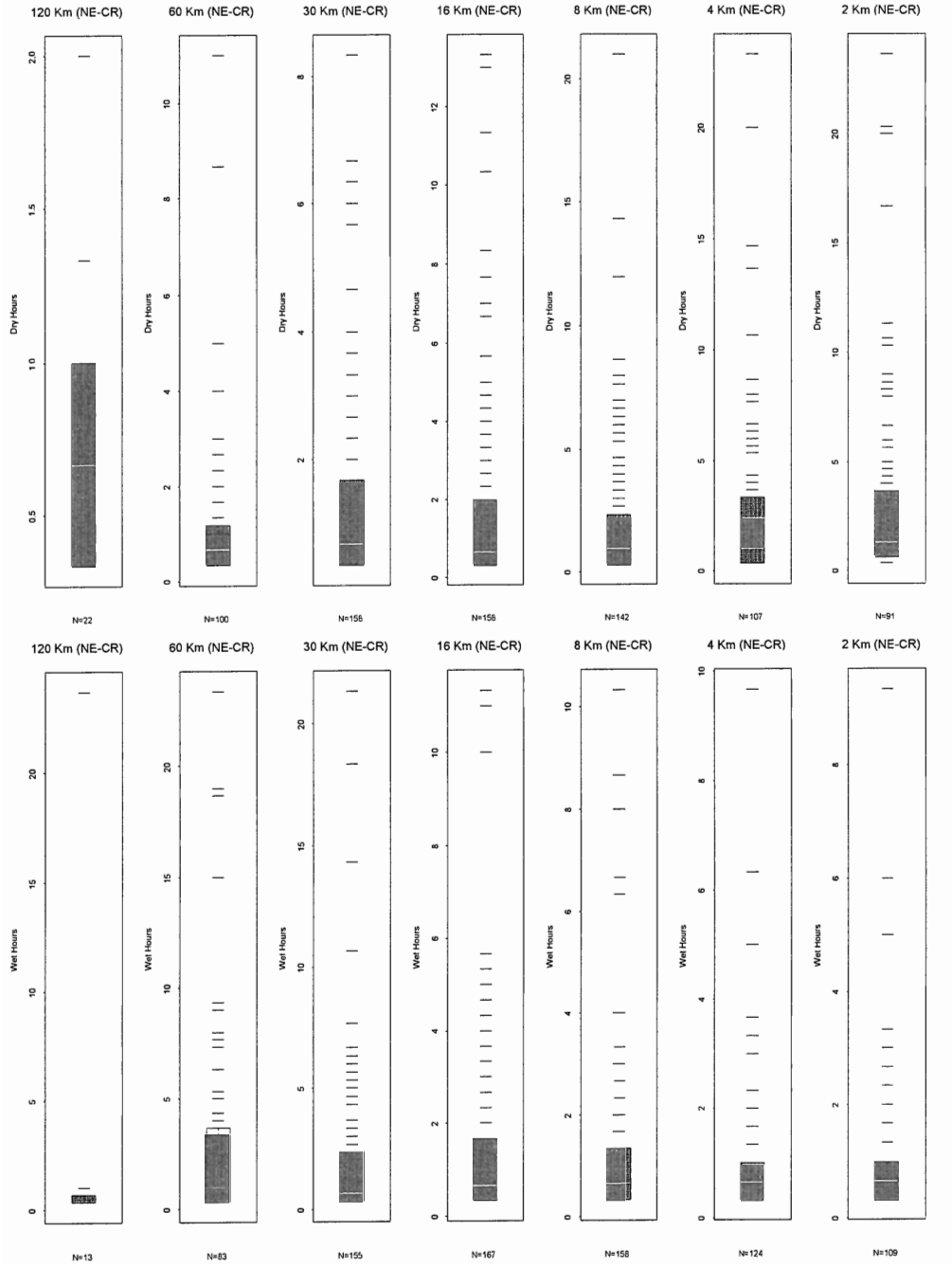

Figure 6: Box-plot summary statistics of dry (top row) and wet (bottom row) spell lengths, after spatial pooling of samples from individual square subregions of the same scale from every design (i.e. box-plots of the 14 sets of "working data"). Each vertical pair of box-plots corresponds to the same spatial scale, and sample sizes of data are denoted by N under each box-plot. The upper and lower sides of each box indicate upper and lower quartiles, the white line inside each box indicates the median or middle quartile, and lines outside each box indicate extreme values in the upper tail of the underlying probability distribution (compare with box-plots in Figure 5).

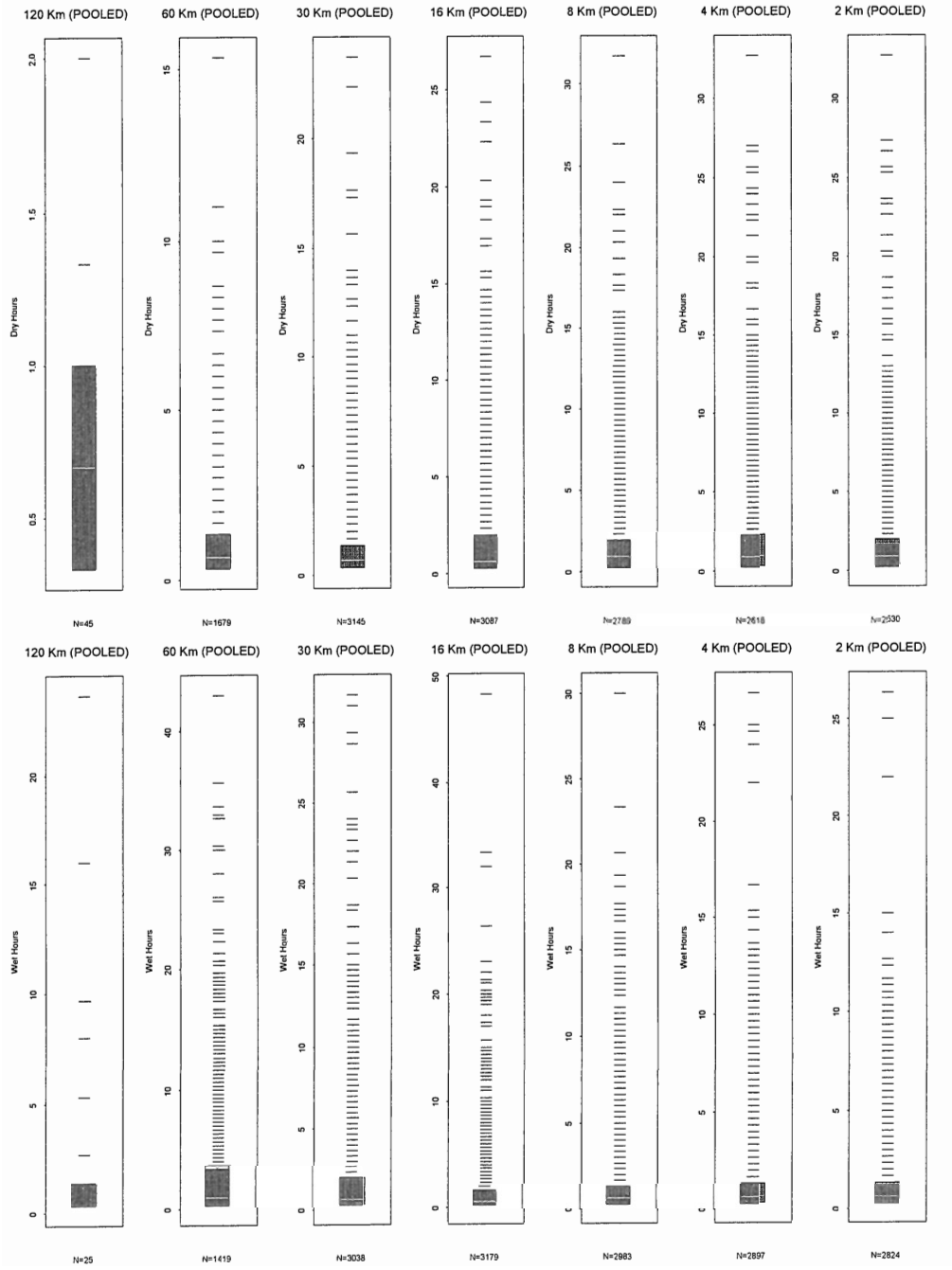

Figure 7: Box-plot summary statistics of p-values from tests of randomness applied to the sampled 25 test sub-regions of each one of the six probed scales (120 Km scale of reference is omitted), for dry (top row) and wet (bottom row) spell lengths. Whiskers above the upper quartile side and below the lower quartile side of each box, mark the largest and smallest p-value obtained respectively.

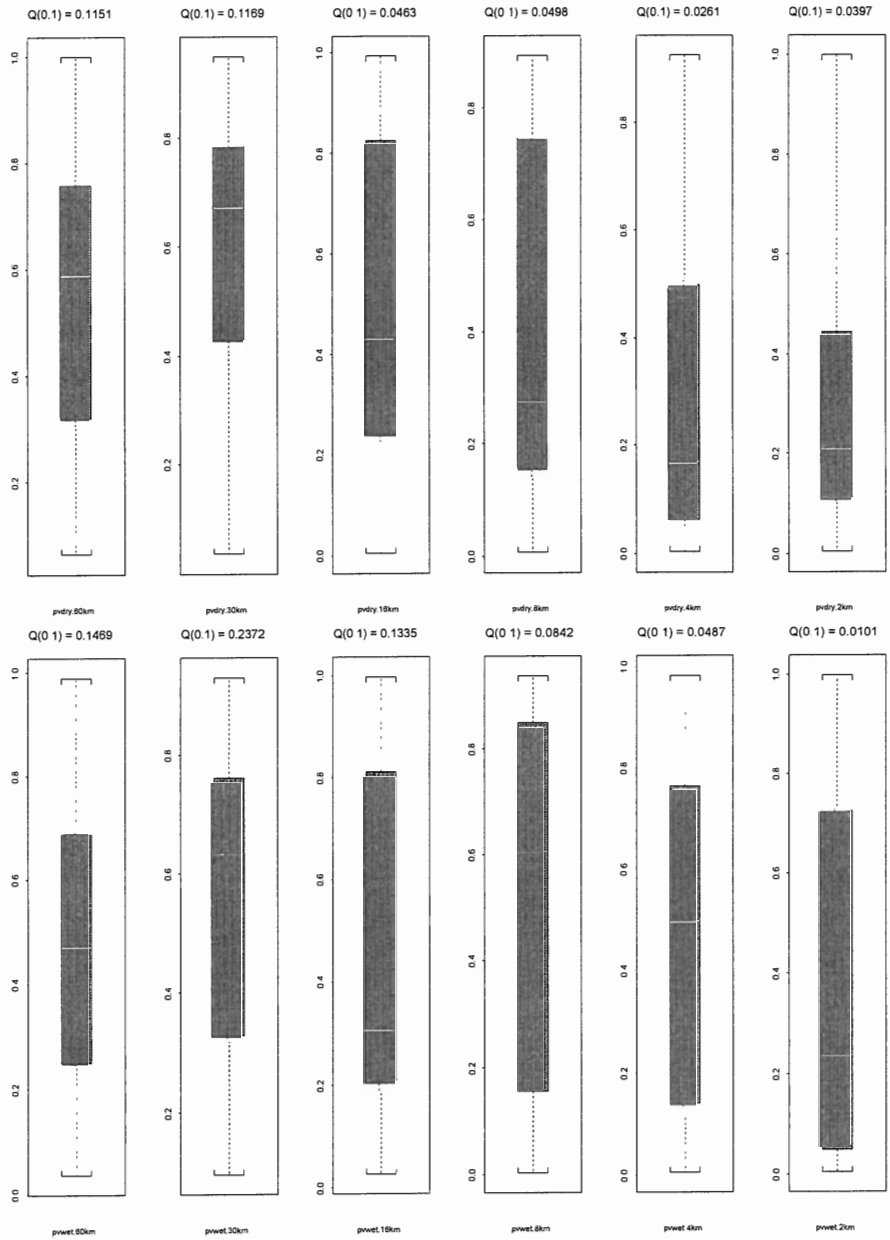

Figure 8: Estimates of the intercept function $\ln B(\lambda)$ and of the slope function $A(\lambda)$ in equation (12), regressed linearly against $\ln \lambda$ in plots (A) and (B) respectively, and estimate of the slope function $\Theta(p)$ in equation (11), regressed linearly against $\ln(1-p)$ in plot (C). Notably, slope and intercept in regression (C) are in perfect agreement with the slopes obtained in regressions (B) and (A) respectively.

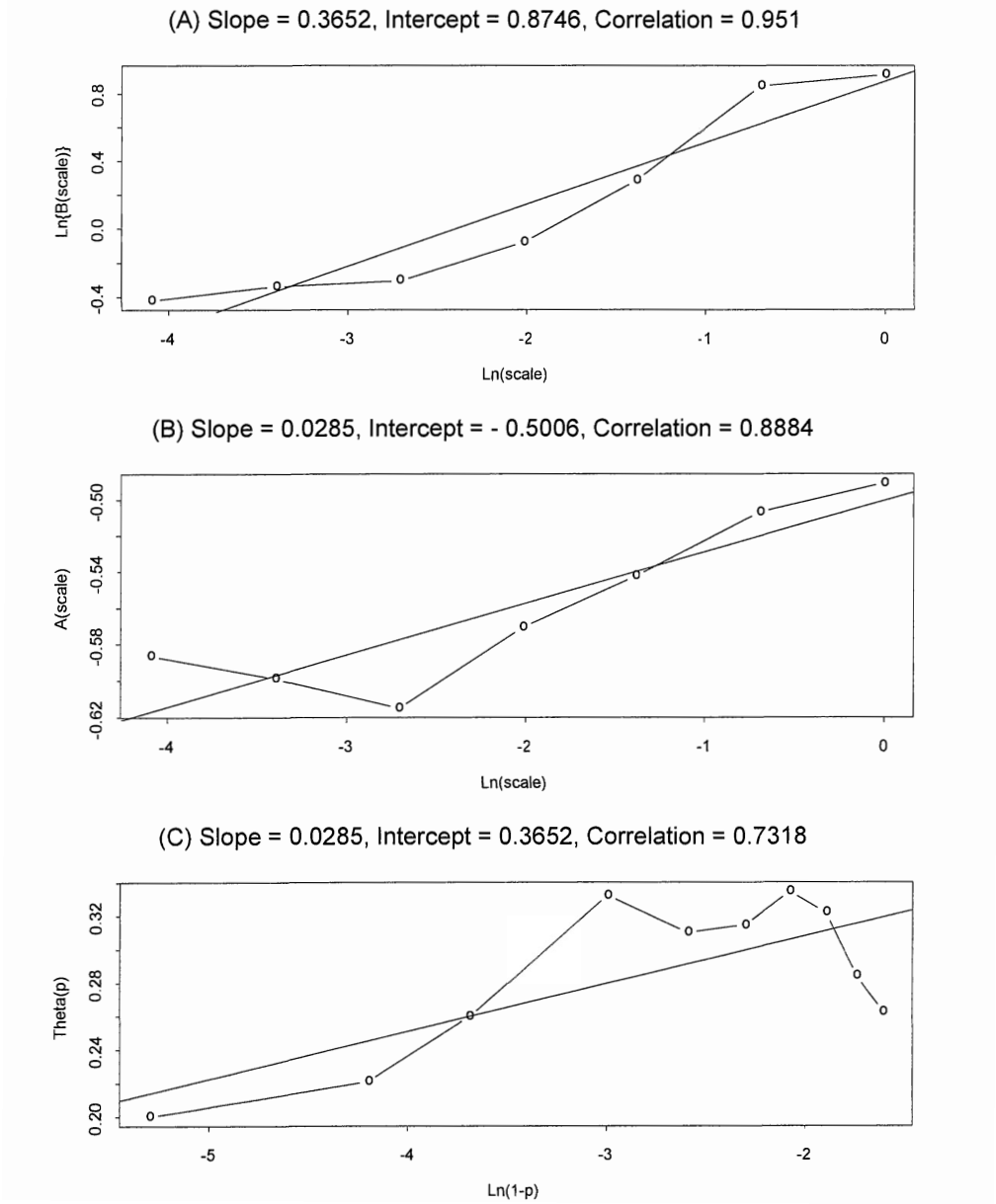

Figure 9: Q-Q-plots of wet duration tail-quantiles predicted by power-law multiscaling according to (13), versus sample estimates of wet duration tail-quantiles, at the same probability levels (0.8, 0.825, 0.85, 0.875, 0.9, 0.925, 0.95, 0.975, 0.985, 0.995), for each one of the probed seven scales (plots A, B, C, D, E, F, G), and collectively across all scales combined (plot H). The correlation reported on each plot is the correlation coefficient obtained from simple linear regression of predicted tail-quantiles against sample ones. The line drawn in each plot is the diagonal through the origin.

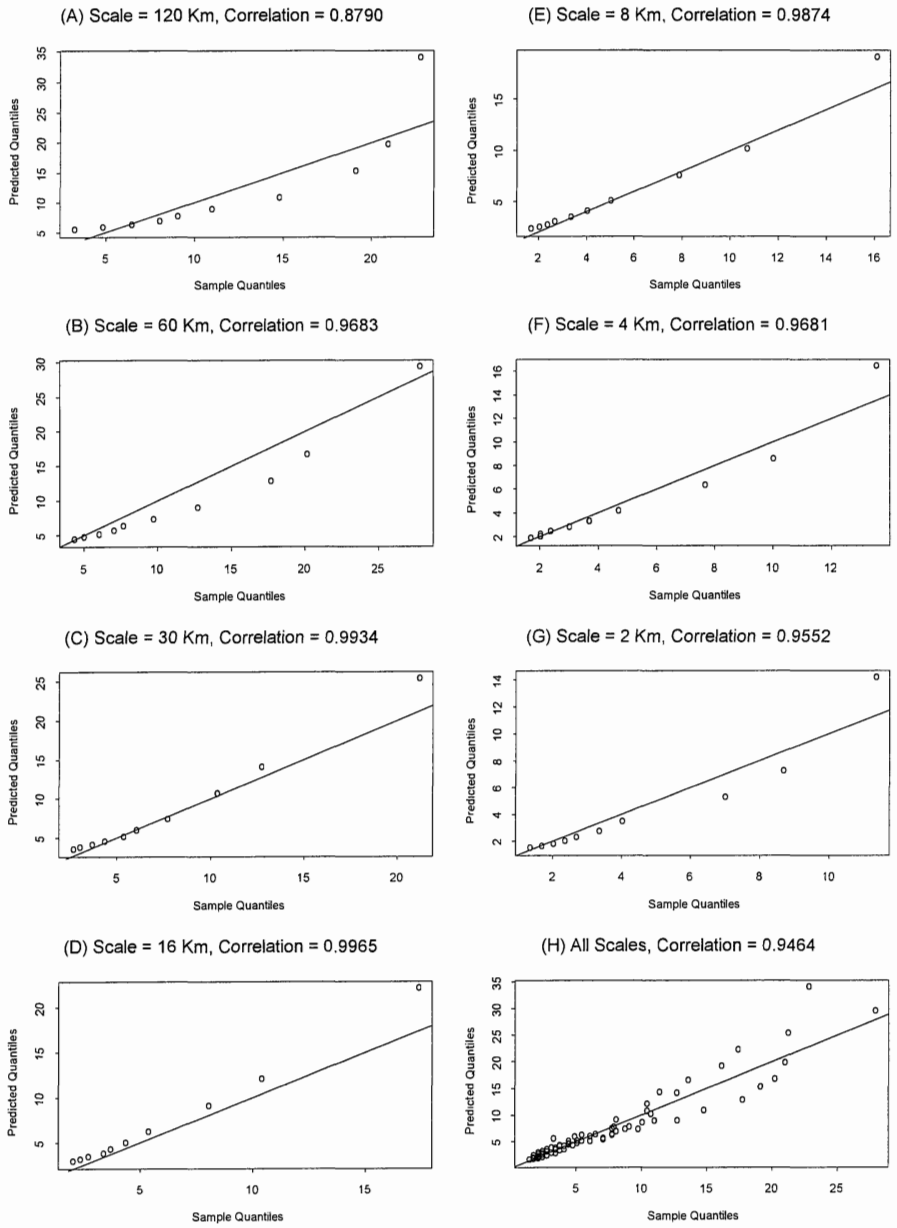

Figure 10: Straight lines fitted by linear regressions of $\ln\left\{m_\lambda^{(w)}(k)/m_1^{(w)}(k)\right\}$ versus $\ln\lambda$ for moment order $k \in \{0.25, 0.5, 0.75, 1, 1.25, 1.5\}$ in (A); Slopes $S(k)$ plotted and linearly regressed versus $k \in \{0.25, 0.5, 0.75, 1, 1.25, 1.5\}$ in (B); and slopes $S(k)$ versus $k \in \{1, 2, 3, 4, 5, 6\}$ in (C).

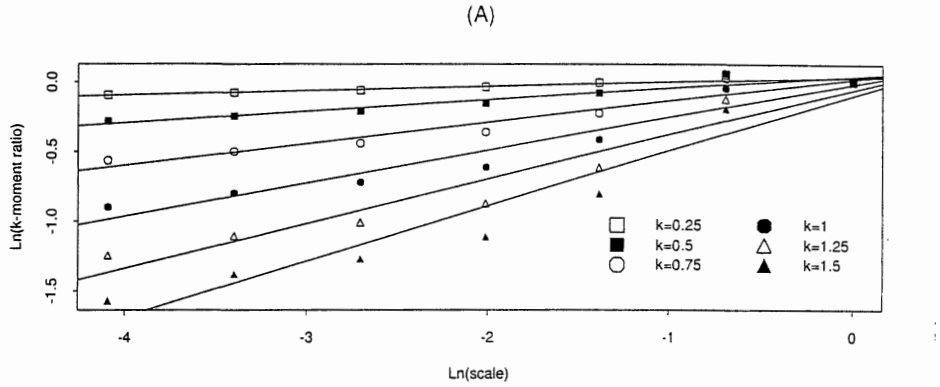

(B) Slope = 0.2990, Intercept = -0.0574, Correlation = 0.9976

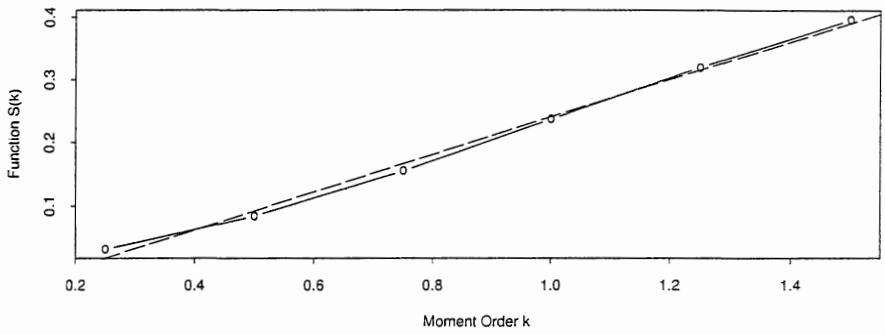

(C) Slope = 0.1215, Intercept = 0.23, Correlation = 0.9425

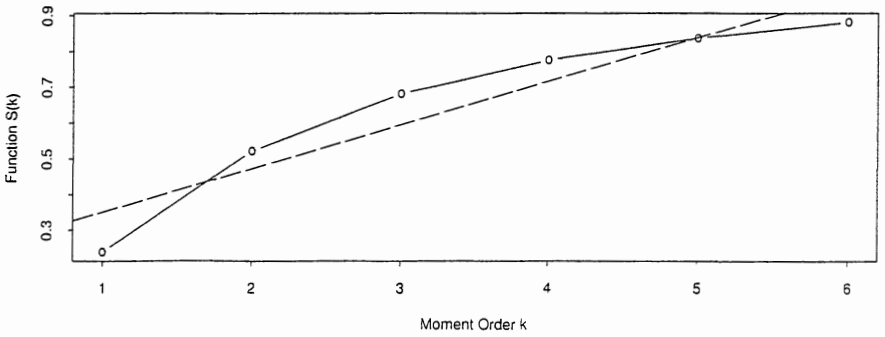

Figure 11: Q-Q-plots of predicted versus sample tail-quantiles of wet duration, for graphical comparison between the power-law multiscaling scenario postulated by (13) and two simple scaling scenaria with scaling exponents 0.2990 and 0.1215, over the entire range of probed scales. The line drawn in each plot is the diagonal through the origin.

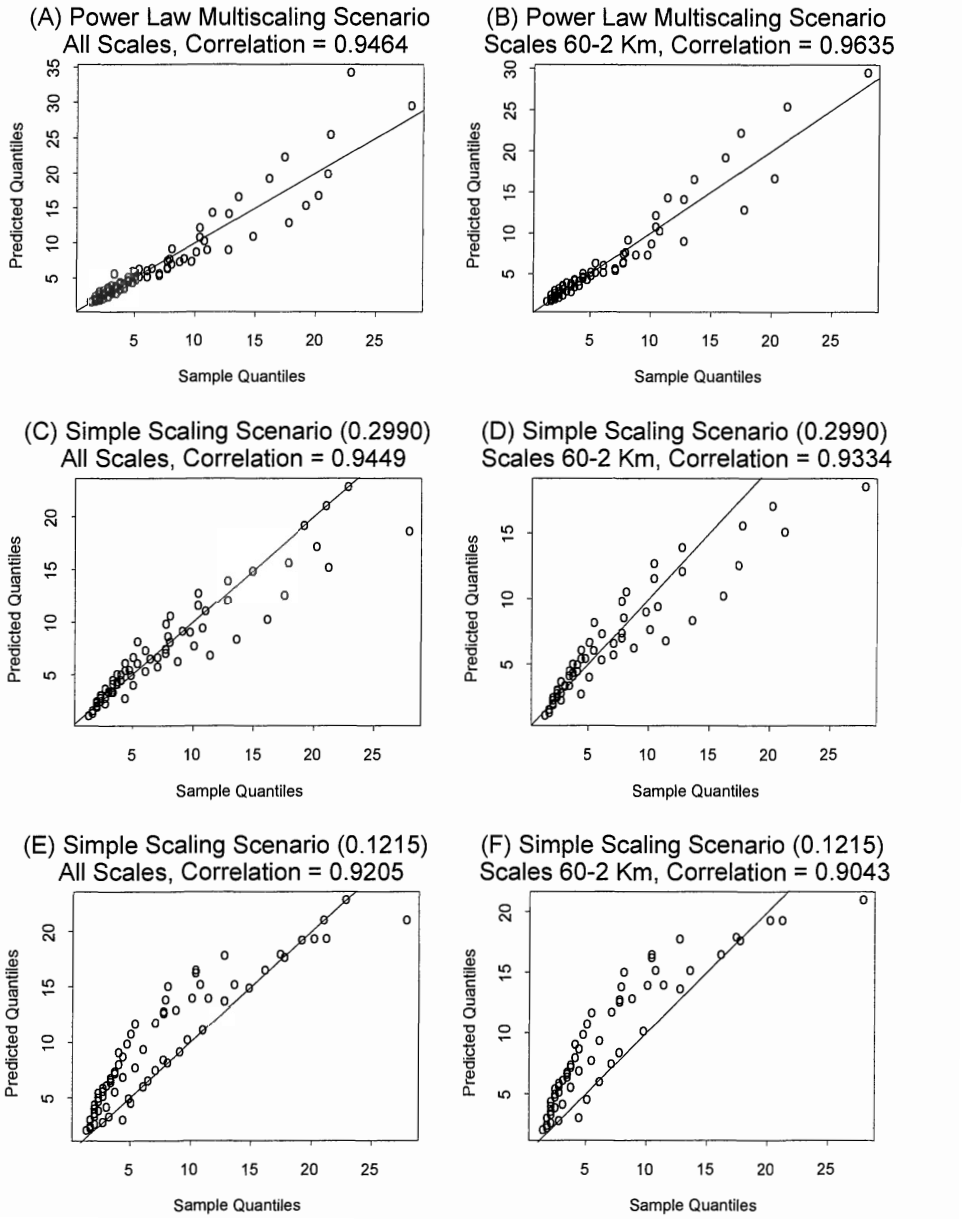

Figure 12: Q-Q-plots of predicted versus sample tail-quantiles of wet duration, for graphical comparison between the power-law multiscaling scenario postulated by (13) and two simple scaling scenaria with scaling exponents 0.1492 and 0.2341, over the 16-to-2 Km lower range of probed scales. The line drawn in each plot is the diagonal through the origin.

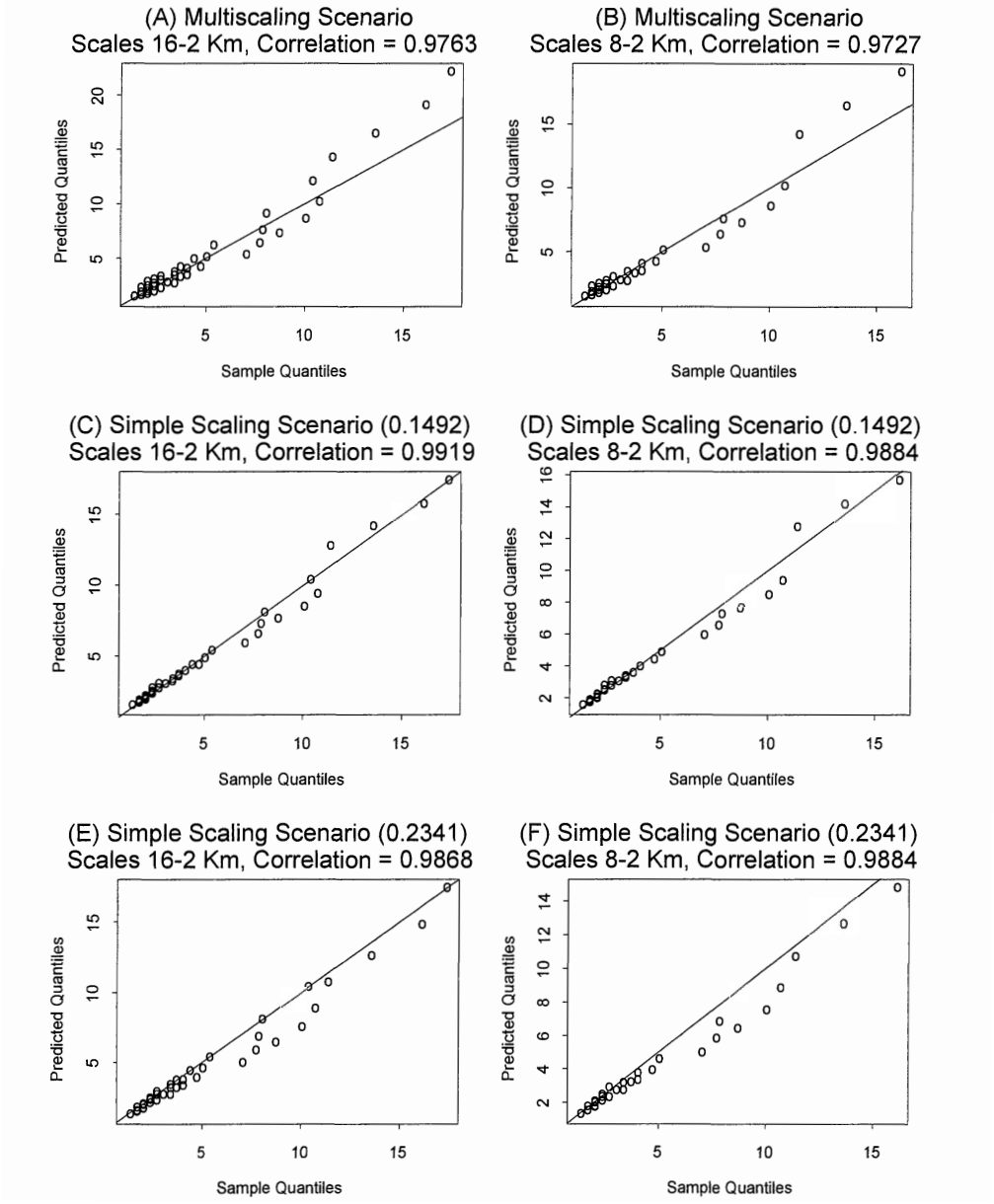

Figure 13: Estimates of the intercept function $\ln B^*(\lambda)$ and of the slope function $A^*(\lambda)$ in equation (18), regressed linearly against λ in plots (A) and (B) respectively, and estimate of the slope function $\Psi(p)$ in equation (17), regressed linearly against $\ln(1-p)$ in plot (C). Notably, slope and intercept in regression (C) are in perfect agreement with the slopes obtained in regressions (B) and (A) respectively.

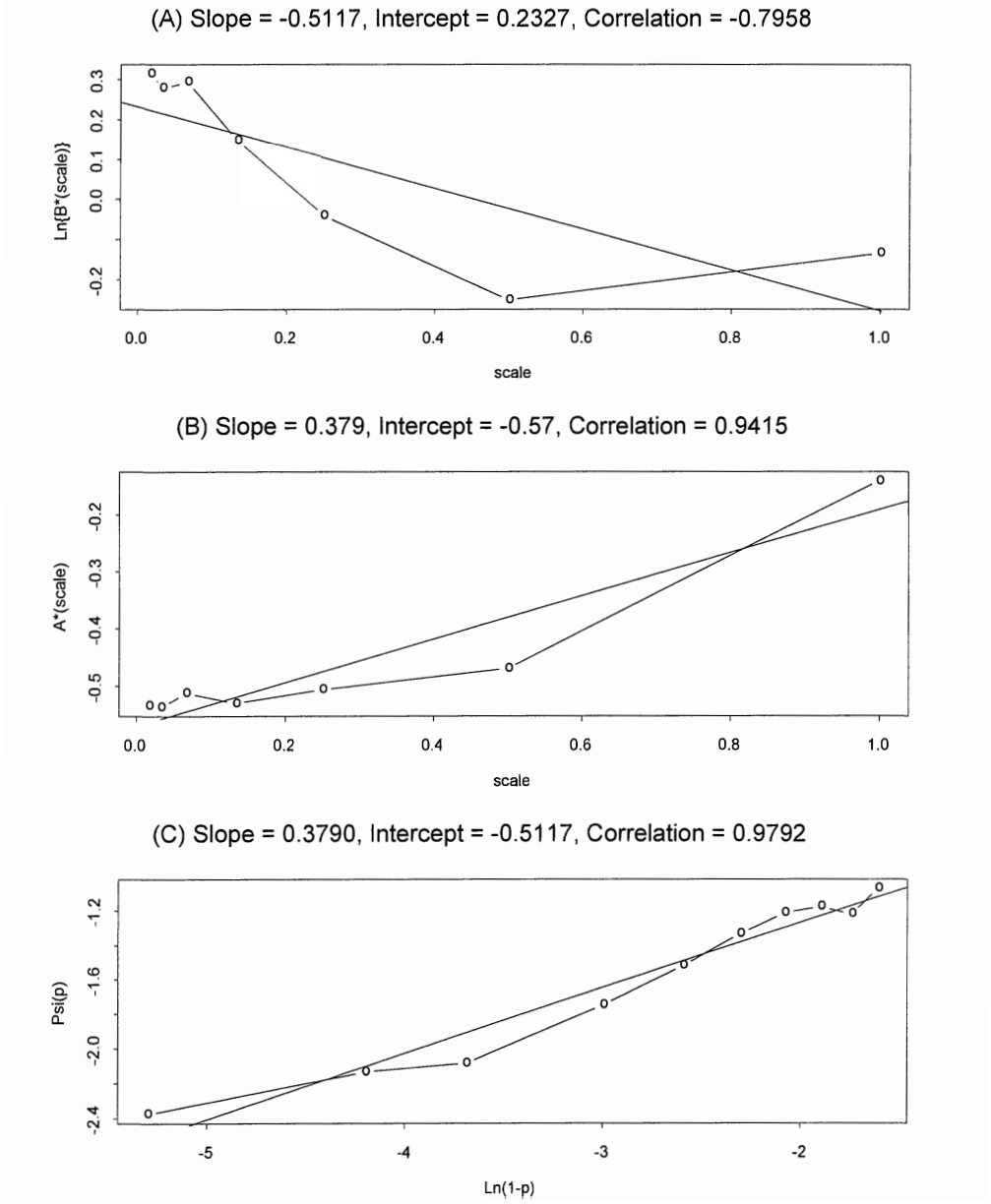

Figure 14:Q-Q-plots of dry duration tail-quantiles predicted by exponential multiscaling, as described by (19), versus sample estimates of dry duration tail-quantiles, at the same probability levels (0.8, 0.825, 0.85, 0.875, 0.9, 0.925, 0.95, 0.975, 0.985, 0.995), for each one of the probed seven scales (plots A, B, C, D, E, F, G), and collectively across all scales combined (plot H). The correlation reported on each plot is the correlation coefficient obtained from simple linear regression of predicted tail-quantiles against sample ones. The line drawn in each plot is the diagonal through the origin.

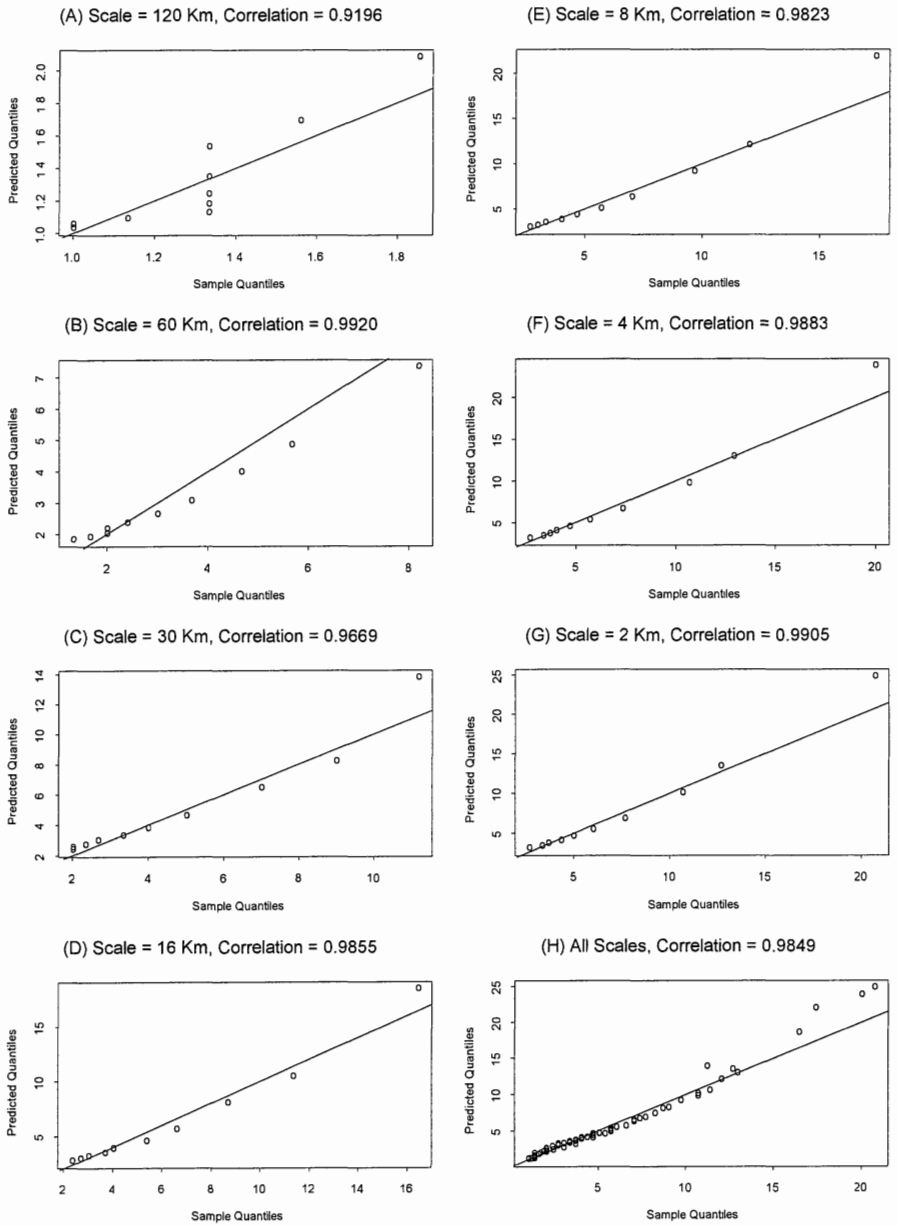

Figure 15: Straight lines fitted by linear regressions of $\ln\left\{m_\lambda^{(d)}(k)/m_1^{(d)}(k)\right\}$ versus $\ln\lambda$ for moments of order $k \in \{0.25, 0.5, 0.75, 1, 1.25, 1.5\}$ in (A); slopes $S^*(k)$ plotted and linearly regressed versus $k \in \{0.25, 0.5, 0.75, 1, 1.25, 1.5\}$ in (B); and slopes $S^*(k)$ versus $k \in \{1, 2, 3, 4, 5, 6\}$ in (C).

(A)

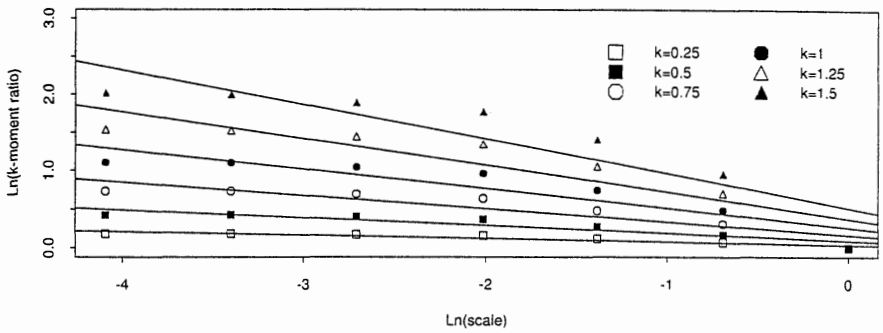

(B) Slope = -0.3292, Intercept = 0.0593, Correlation = -0.9944

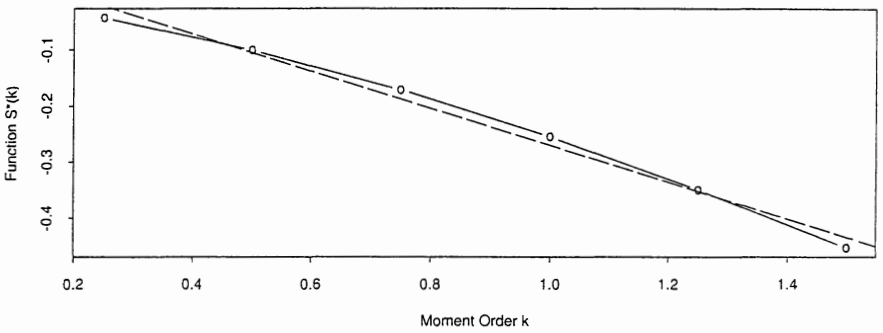

(C) Slope = -0.5036, Intercept = 0.2962, Correlation = -0.9994

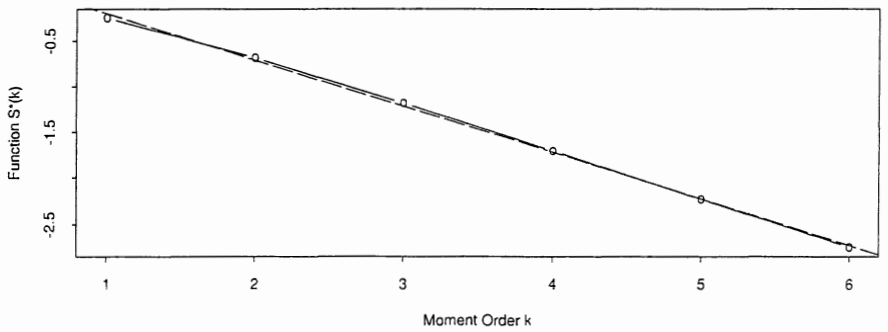

Figure 16: Q-Q-plots of predicted versus sample tail-quantiles of dry duration, for graphical comparison between the power-law multiscaling scenario postulated by (19) and two simple scaling scenaria with scaling exponents -0.3292 and -0.5036, over the entire range of probed scales. The line drawn in each plot is the diagonal through the origin.

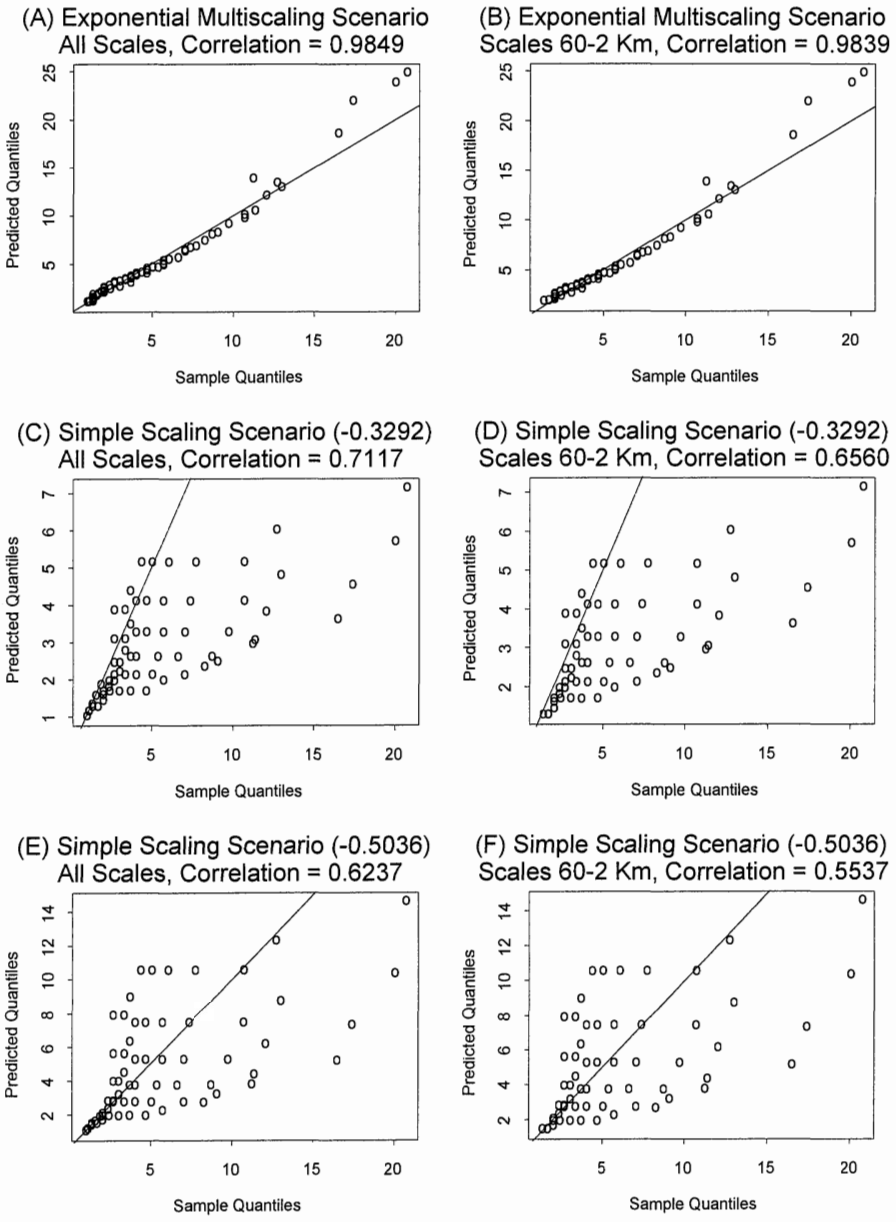

Figure 17: Straight lines fitted by linear regressions of $\ln\left\{m_\lambda^{(d)}(k)/m_1^{(d)}(k)\right\}$ versus $\lambda-1$ for moments of order $k \in \{0.25, 0.5, 0.75, 1, 1.25, 1.5\}$ in (A); slopes $H(k)$ plotted and linearly regressed versus $k \in \{0.25, 0.5, 0.75, 1, 1.25, 1.5\}$ in (B); and slopes $H(k)$ versus $k \in \{1, 2, 3, 4, 5, 6\}$ in (C).

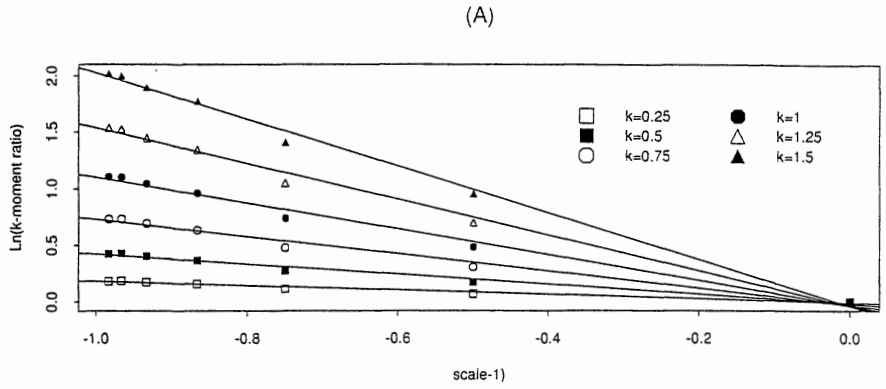

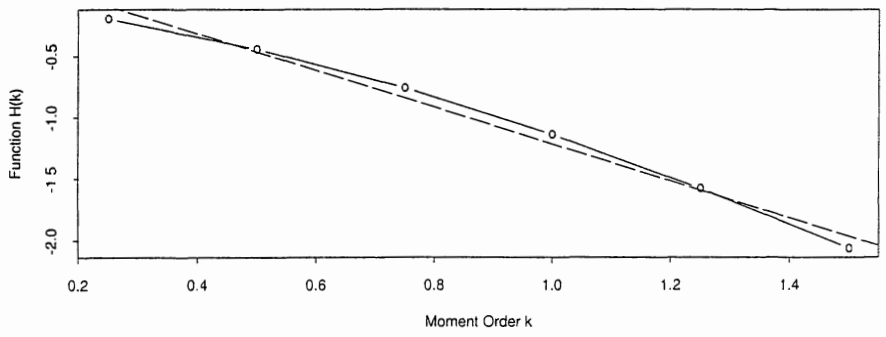

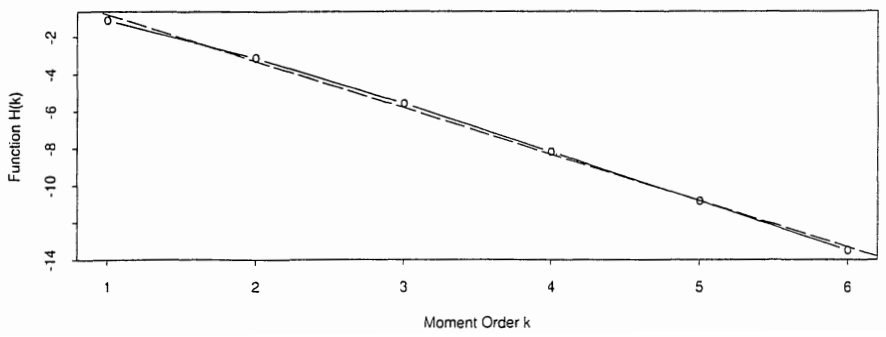

Figure 18:Q-Q-plots of predicted versus sample tail-quantiles of dry duration, for graphical comparison between the exponential multiscaling scenario postulated by (19) and two simple scaling scenaria with scaling exponents 0.1492 and 0.2341, over the 16-to-2 Km lower range of probed scales.The line drawn in each plot is the diagonal through the origin.

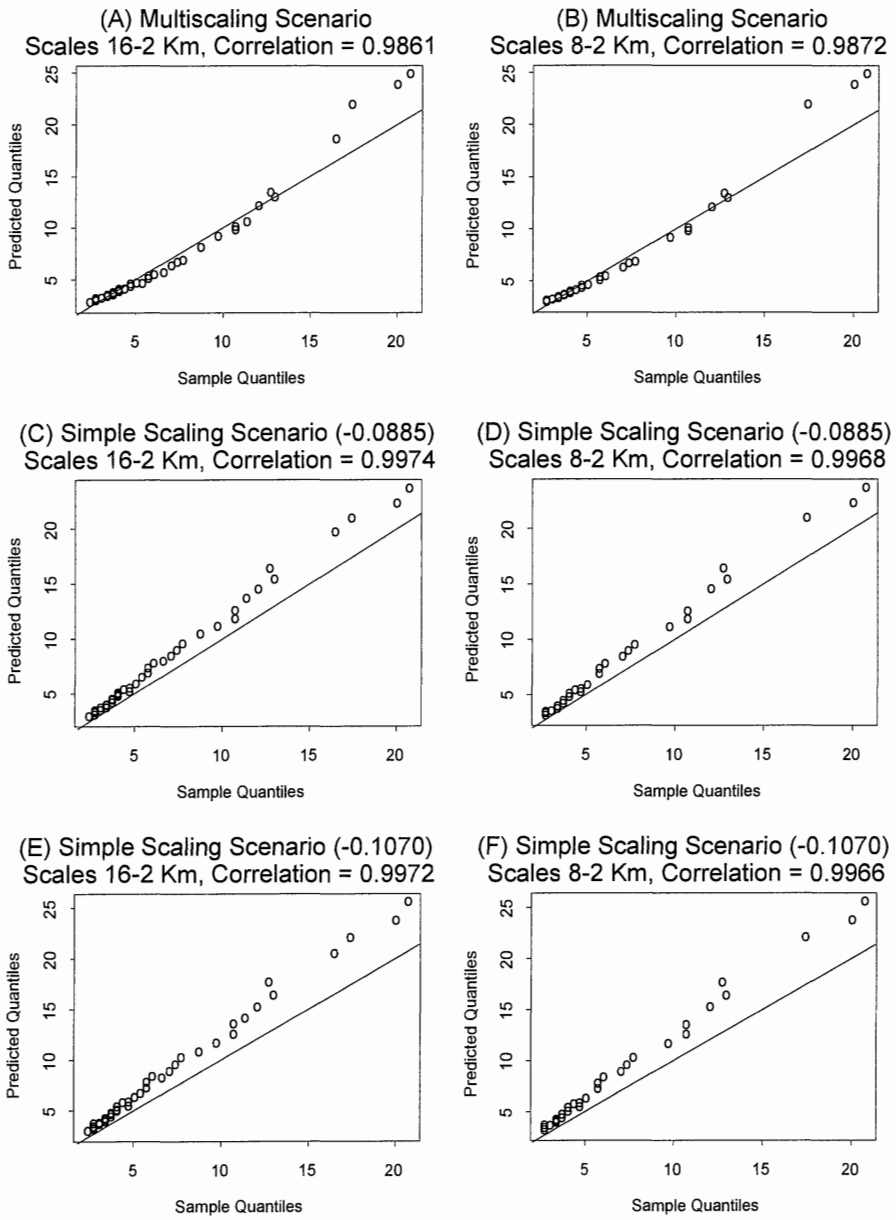

Figure 19: Histogram plots of box-counting sample estimates of capacity fractal dimension of wet residence time for the probed scales.

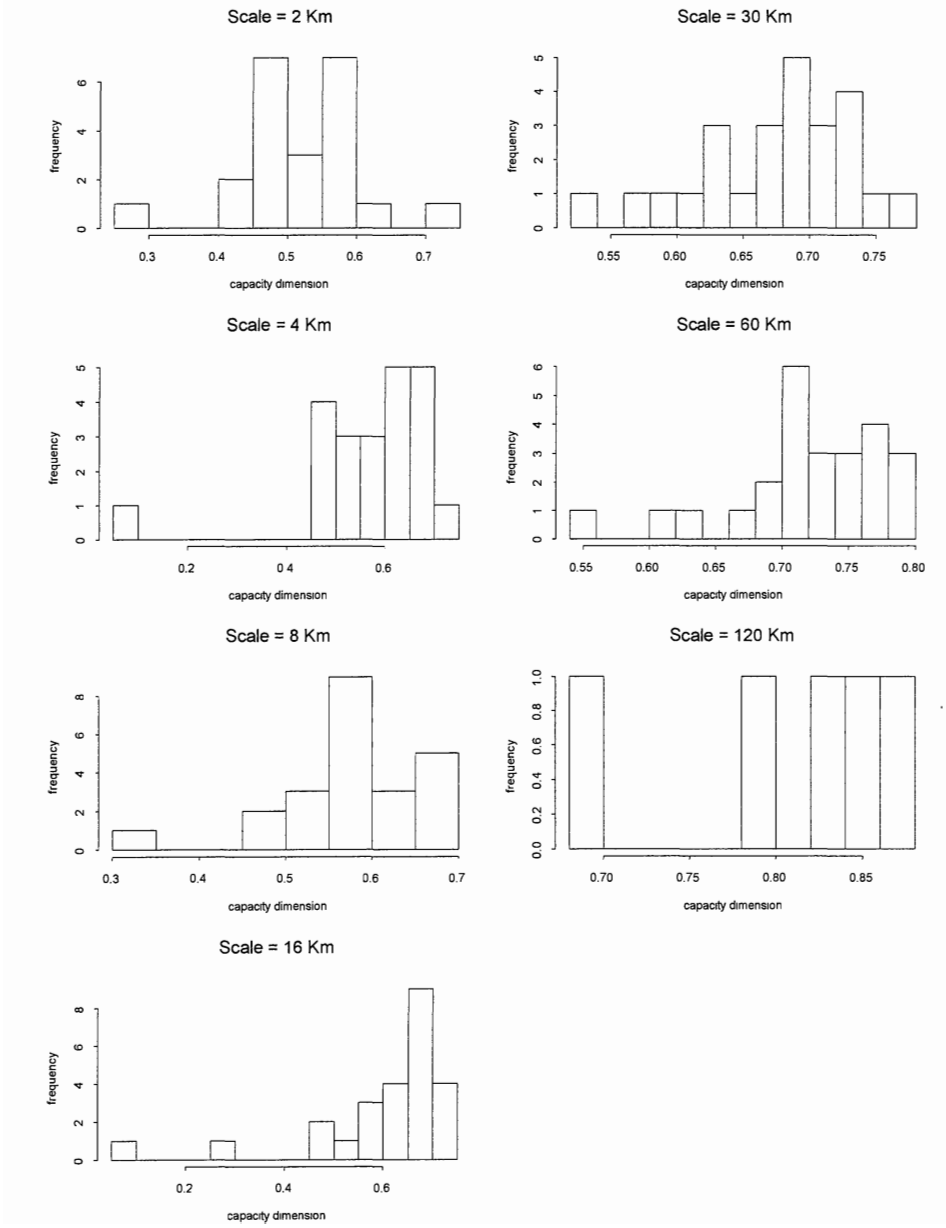

Figure 20: Plot of estimates of the differences $1/\Delta_\lambda - 1/\Delta_1$, for median and mean estimates of fractal dimension, versus their predicted values $0.379 \cdot (1-\lambda)$ according to (26). The line drawn in each plot is the diagonal through the origin.